

Attention-Aided MMSE for OFDM Channel Estimation: Learning Linear Filters with Attention

TaeJun Ha, Chaehyun Jung, Hyeonuk Kim, Jeongwoo Park, and Jeonghun Park

Abstract—In orthogonal frequency division multiplexing (OFDM), accurate channel estimation is crucial. Classical signal processing based approaches, such as minimum mean-squared error (MMSE) estimation, often require second-order statistics that are difficult to obtain in practice. Recent deep neural networks based methods have been introduced to address this; yet they often suffer from high inference complexity. This paper proposes an Attention-aided MMSE (A-MMSE), a novel model-based DNN framework that learns the optimal MMSE filter via the Attention Transformer. Once trained, the A-MMSE estimates the channel through a single linear operation for channel estimation, eliminating nonlinear activations during inference and thus reducing computational complexity. To enhance the learning efficiency of the A-MMSE, we develop a two-stage Attention encoder, designed to effectively capture the channel correlation structure. Additionally, a rank-adaptive extension of the proposed A-MMSE allows flexible trade-offs between complexity and channel estimation accuracy. Extensive simulations with 3GPP TDL channel models demonstrate that the proposed A-MMSE consistently outperforms other baseline methods in terms of normalized MSE across a wide range of signal-to-noise ratio (SNR) conditions. In particular, the A-MMSE and its rank-adaptive extension establish a new frontier in the performance-complexity trade-off, providing a powerful yet highly efficient solution for practical channel estimation.

Index Terms—Orthogonal frequency division multiplexing (OFDM), Channel estimation, Minimum mean-squared error (MMSE), Attention Transformer, Deep learning

I. INTRODUCTION

Orthogonal frequency division multiplexing (OFDM) is a foundational waveform in modern wireless communication systems. OFDM was initially adopted in earlier standards such as Wi-Fi (IEEE 802.11), WiMAX, and was later introduced into the 3GPP-based cellular ecosystem with LTE. This adoption paved the way for OFDM's continued prominence in 5G [1], [2] and its expected role in future 6G technologies [3].

This work was supported in part by the 6GARROW project which has received funding from the Smart Networks and Services Joint Undertaking (SNS JU) under the European Union's Horizon Europe research and innovation program under Grant Agreement No 101192194 from the Institute for Information & Communications Technology Promotion (IITP) grant funded by the Korean government (MSIT) (No. RS-2024-00435652), in part by Institute of Information & communications Technology Planning & Evaluation (IITP) grant funded by the Korea government (MSIT) (No. RS-2024-00395824, Development of Cloud virtualized RAN (vRAN) system supporting upper-midband), in part by the Institute of Information & Communications Technology Planning & Evaluation(IITP)-Digital Innovation Talent Short-Term Intensive program grant funded by the Korea government (MSIT) (No. RS-2024-00404972).

The authors are with School of Electrical and Electronic Engineering, Yonsei University, South Korea (e-mail: tjha@yonsei.ac.kr, jch0624@yonsei.ac.kr, garksill@yonsei.ac.kr, simyffff@yonsei.ac.kr, jhpark@yonsei.ac.kr)

One of the critical problems in OFDM is channel estimation, which is essential for enabling coherent detection. The goal of OFDM channel estimation is to accurately estimate the channel state information for each subcarrier using noisy pilot symbols. A classical solution for the OFDM channel estimation involves signal processing (SP)-based approaches, including least square (LS) and minimum mean-squared error (MMSE) estimation methods [4], [5]. LS is simple to implement, but its performance is limited because it cannot incorporate prior OFDM channel statistics. MMSE, in contrast, requires second-order statistics, such as noise variance and correlation across subcarriers, which are difficult to obtain accurately in practical scenarios [6].

Beyond traditional SP-based approaches, sensing-aided channel estimation has emerged within the integrated sensing and communication (ISAC) frameworks [7], [8]. These methods leverage communication signal echoes to extract sensing parameters, which then serve as prior information for channel refinement. Despite showing promise in exploiting communication-sensing synergy, these approaches require additional computational resources for sensing processing.

Recently, inspired by the remarkable success of deep neural networks (DNNs) across various engineering fields, DNN-aided channel estimation for OFDM has gained considerable attention. DNNs, as pre-trained neural network models, can effectively capture complex data relationships without explicit prior statistical knowledge. Leveraging this data-driven approach, several prior works have explored DNN-aided OFDM channel estimation strategies. In [9], an OFDM channel slot was treated as image data. Based on this, a super-resolution network and a denoising neural network were simultaneously employed to estimate the OFDM channel (i.e., ChannelNet). In [10], using a similar modeling approach to [9], ReEsNet [10] was proposed, where a residual learning-based DNN was used to reconstruct the OFDM channel. This method achieves lower computational cost and higher accuracy than [9]. In [11], a residual convolutional network combined with bilinear interpolation was proposed for OFDM channel estimation, offering enhanced flexibility to varying pilot patterns and reduced complexity. Beyond deterministic models, [12] optimized a deep generative model using compressive pilot measurements for high-dimensional channel estimation. This method leverages learned priors to reduce pilot overhead and surpass traditional sparse recovery techniques.

In particular, with the advent of the Attention Transformer architecture [13], some recent works investigated Transformer models as a compelling solution for wireless channel estimation problems, owing to their representational capacity. In [14],

super-resolution techniques were integrated with an Attention-based encoder-decoder framework to enhance OFDM channel estimation accuracy. In [15], Channelformer was developed, where an Attention-based encoder-decoder neural architecture was designed to incorporate input precoding. A common structure in prior studies using DNNs for channel estimation [9]–[12], [14], [15] is the use of a pre-trained neural network that directly maps noisy pilot signals to the estimated channel matrix, as illustrated in the left panel of Fig. 1.

Despite their significant advantages over classical SP-based channel estimation methods, existing DNN-based approaches have several limitations. We summarize these as follows.

- **Computational overhead:** Typically, DNN-based models involve a large number of parameters (approximately 53,000 for ReEsNet [10] and 110,000 for Channelformer [15]), leading to significant computational and memory overhead per channel estimation. Furthermore, several nonlinear operations are used (e.g., ReLU [16], tanh [17], ELU [18], and pooling [19]), limiting hardware acceleration effectiveness. These nonlinearities, although essential for model expressiveness, may introduce additional computational overhead and pose challenges related to inference complexity and practical implementation.
- **Limited interpretability:** Existing DNN-based approaches are typically applied directly to OFDM channel estimation in a purely data-driven manner, without incorporating domain knowledge derived from mathematical models. However, studies such as [20], [21] showed that integrating domain-specific insights into neural network design can lead to notable performance gains over purely data-driven methods. This implies that considerable potential remains to further push performance boundaries by leveraging domain-specific insights.
- **Lack of flexibility:** For practical deployment, it is often desirable for channel estimation methods to adaptively adjust computational load. For example, assuming a scenario where a user has severely constrained processing resources, the estimator should be able to reduce its complexity by adjusting the number of parameters. However, most existing DNN-based approaches lack this adaptability, as they provide no explicit mechanisms to control the model size or computational cost within the DNN architecture.

We note that these limitations primarily arise from employing DNNs as end-to-end channel estimators, where the model learns a direct mapping from noisy pilot signals to channel estimates solely based on data.

To address the challenges of purely data-driven approaches, recent research has actively explored the concept of model-based DNNs [22]. The core idea is to leverage a hybrid method that combines classical SP-based approaches and data-driven DNN-based approaches, thereby harnessing the advantages of both methodologies, i.e., powerful learning capability and mathematical interpretability. For instance, [23] proposed KalmanNet, where the Kalman gain matrix is learned using recurrent neural network architectures such as long short-term memory (LSTM) [24] or gated recurrent units (GRU) [25],

while retaining the recursive update structure of the classical Kalman filtering algorithm [26]. Thanks to its hybrid design, KalmanNet [23] effectively address the state estimation problem, even with partially known state models. Subsequently, several extensions were proposed, including [27]–[30]. In parallel, model-based DNN approaches have been widely applied to various tasks, such as multiple-input multiple-output (MIMO) beamforming design [31], [32], and MIMO detection [21], [33]. However, to the best of our knowledge, no model-based DNN framework has been explored for OFDM channel estimation. This work addresses this notable gap by devising a novel channel estimation method that leverages not only the learning capability of DNNs but also domain knowledge from classical SP-based approaches.

In this paper, we propose an Attention-aided MMSE (A-MMSE) method for OFDM channel estimation. The key idea is to exploit the Attention Transformer architecture to learn linear channel estimation filter coefficients, rather than directly estimating the OFDM channel outputs using DNNs. The fundamental difference between conventional DNN-based approaches and the proposed method is illustrated in Fig. 1. Once the linear filters are trained using the Attention Transformer, the proposed A-MMSE performs channel estimation solely by relying on a linear process, effectively decoupling the estimation mechanism from the learning procedure. Building on the linear estimation structure of the A-MMSE, we further extend it by enabling the rank-adaptive capability, referred to as the rank-adaptive A-MMSE (RA-A-MMSE). By adjusting the rank of the RA-A-MMSE estimation filter matrix, we achieve additional reductions in computational overhead with minimal loss in channel estimation accuracy.

Beyond the A-MMSE architecture, we also develop a novel two-stage Attention encoder to further enhance the channel estimation performance. Specifically, we first observe that the OFDM channel’s correlation matrix can be effectively decomposed into frequency and temporal domain correlations. Building on this insight, our two-stage Attention encoder consists of Frequency Encoder and Temporal Encoder, each designed to capture the corresponding correlation structure. In particular, the Frequency Encoder exploits a Multi-Head Self-Attention mechanism combined with a linear embedding, whose dimension matches the number of subcarriers. Subsequently, the Frequency Encoder’s output features are projected to the Temporal Encoder, which also leverages Multi-Head Self-Attention with an embedding dimension matching the total number of OFDM channel elements. By sequentially integrating the Frequency and Temporal Attention encoder blocks, our method effectively reflects complementary relationships across the frequency and temporal domains, extracting highly relevant latent features. These refined features are then decoded by a residual fully-connected network, precisely mapping them to the linear filter coefficients of the proposed A-MMSE method. Thanks to the two-stage Attention structure, OFDM channels’ inherent correlation characteristics are effectively incorporated in a form particularly suitable for A-MMSE filter design, significantly enhancing the overall estimation performance.

Via numerical simulations across diverse 3GPP TDL scenarios, we show that the proposed A-MMSE and RA-A-MMSE

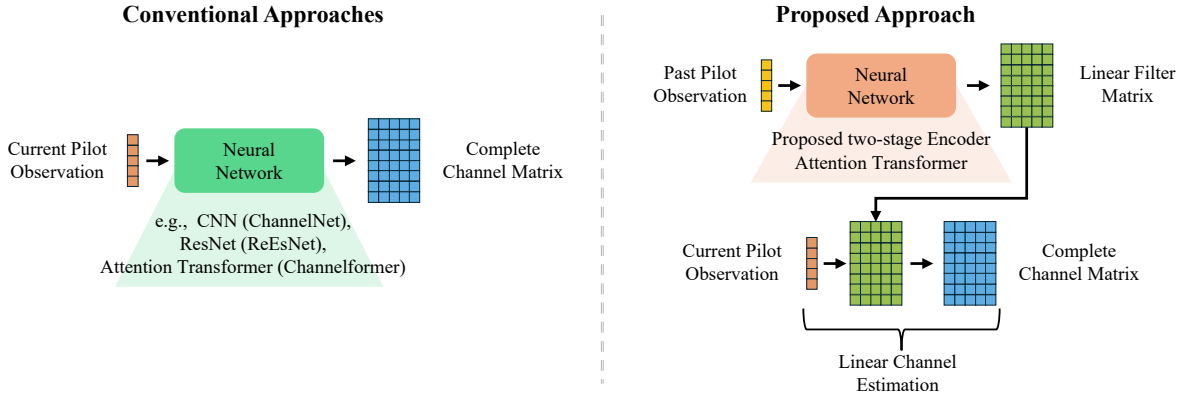


Fig. 1. Comparison of OFDM channel estimation structure: conventional approaches vs. the proposed A-MMSE approach.

significantly outperform traditional SP-based approaches (e.g., LS and MMSE) and recent DNN-based approaches (e.g., ChannelNet [9] and Channelformer [15]) in terms of channel estimation accuracy. In particular, the A-MMSE achieves approximately 43% lower normalized MSE (NMSE) compared to conventional MMSE. We attribute these performance gains to the Attention Transformer’s ability to effectively capture nonstationary channel statistics, even under challenging high-mobility and frequency-selective fading conditions. Comparing to Channelformer, the A-MMSE achieves approximately 48% lower NMSE. We note that these gain stem from our novel two-stage Attention encoder architecture, where frequency domain features are first extracted and subsequently refined through temporal correlation modeling. These channel estimation improvements directly translate to symbol detection performance gains, with A-MMSE achieving 13.1% and 26.6% lower bit error rate (BER) compared to MMSE and Channelformer respectively in the challenging mmWave scenario at 25 dB SNR. Furthermore, the proposed method surpasses recent sensing-aided approaches [7], achieving up to a 35% lower NMSE in high-mobility scenarios without the added complexity of echo signal processing. Moreover, the RA-A-MMSE further reduces computational complexity through adaptive rank reduction, maintaining over 99.6% of the performance achieved by the full-rank A-MMSE. As a result, the RA-A-MMSE requires only 1.5% of the computational complexity of Channelformer or MMSE (i.e., a 98.5% reduction), while achieving approximately 36% lower NMSE. The proposed methods also exhibit strong robustness to signal-to-ratio (SNR) mismatch, retaining nearly full performance ($\geq 98.1\%$) across a wide range of unseen SNR conditions. This underscores the practical efficiency and suitability of the proposed method for real-world 5G/6G implementations.

In summary, the proposed A-MMSE method offers several advantages over existing approaches. First, the proposed A-MMSE with novel two-stage Attention encoder effectively incorporates the OFDM channel correlation structure, thereby significantly improving channel estimation accuracy and robustness, achieving around 43% and 48% lower NMSE compared to MMSE and Channelformer, respectively. Second, once trained, the A-MMSE employs purely linear computa-

tions for OFDM channel estimation, significantly reducing computational complexity compared to conventional DNN-based methods that heavily rely on numerous nonlinear operations. Especially, the RA-A-MMSE dynamically adjusts its computational complexity according to available hardware resources, requiring 99.8% fewer computations than the average of conventional DNN-based methods. This enables both efficient and flexible implementation in practical systems. Third, the A-MMSE also achieves up to 35% lower NMSE than recent sensing-aided method in high-mobility scenarios, without the need for additional sensing signal processing.

The rest of the paper is organized as follows. Section II describes the basic system model, and Section III introduces the conventional channel estimation methods including the SP-based approaches and the DNN-based approaches. In what follows, Section IV presents the main concept of the proposed A-MMSE method, and Section V further extends it to the RA-A-MMSE. Numerical results are provided in Section VI, and Section VII concludes the paper.

Notations: We denote transpose by $(\cdot)^T$, Hermitian transpose by $(\cdot)^H$, complex conjugate by $(\cdot)^*$, column-wise vectorization by $\text{vec}(\cdot)$, real and imaginary parts of a complex quantity by $\Re(\cdot)$ and $\Im(\cdot)$, the magnitude by $|\cdot|$, and the Euclidean and Frobenius norms by $\|\cdot\|_2$ and $\|\cdot\|_F$, respectively. Element-wise (Hadamard) multiplication is denoted by \circ , the Kronecker product by \otimes , and statistical expectation is written as $\mathbb{E}[\cdot]$. The set difference is denoted by \setminus , horizontal (row-wise) stacking by $[\cdot, \cdot]$, and vertical (column-wise) stacking by $[\cdot; \cdot]$.

II. SYSTEM MODEL

In this section, we explain the system model used in this paper. We focus on a single OFDM slot with M OFDM symbols, each comprising N subcarriers, for a total of NM resource elements. The channel’s frequency response corresponding to the n -th subcarrier and the m -th symbol is denoted as $H[n, m]$. Assuming that the cyclic-prefix (CP) is removed, the received signal model in the frequency domain is given by

$$Y[n, m] = H[n, m]X[n, m] + Z[n, m], \quad (n, m) \in \mathcal{T}, \quad (1)$$

where $X[n, m]$ is the transmitted signal, $Z[n, m]$ is the additive Gaussian noise, and \mathcal{T} denotes the set of all resource elements. We denote by \mathcal{P} the set of indices corresponding to the pilot signals, where $|\mathcal{P}| = L$. This indicates that a total of L pilot symbols are used for channel estimation. Accordingly, $X[n, m]$ is known to the receiver for $(n, m) \in \mathcal{P}$. Let \mathcal{D} be the set of indices corresponding to the data signals, such that $\mathcal{P} \cup \mathcal{D} = \mathcal{T}$. For notational convenience, we define \mathbf{H} as the channel matrix whose (n, m) -th element is $H[n, m]$, and similarly for \mathbf{Y} , \mathbf{X} , and \mathbf{Z} . Accordingly, the signal model (1) is equivalently expressed as

$$\mathbf{Y} = \mathbf{H} \circ \mathbf{X} + \mathbf{Z}. \quad (2)$$

5G NR specifies the configuration of OFDM slots. For instance, in a standard OFDM resource block configuration with a normal cyclic prefix (CP) and subcarrier spacing of 30 kHz, each resource block comprises 12 subcarriers in frequency and 14 OFDM symbols in time. In this structure, with a typical Type-A demodulation reference signal (DM-RS) configuration for the physical downlink shared channel (PDSCH), the DM-RS can be inserted into two OFDM symbols, commonly at symbol indices 2 and 11, depending on the configured DM-RS pattern. All resource elements in other symbols are typically allocated for data. We generally follow 5G NR PDSCH configuration setup, but note that our approach is also applicable to arbitrary configurations beyond this standard setting.

The OFDM channel estimation problem aims to estimate the channel matrix \mathbf{H} , denoted by $\hat{\mathbf{H}}$, given the observations \mathbf{Y} and the known pilot signal $X[n, m]$ at $(n, m) \in \mathcal{P}$. The MSE is commonly adopted as the performance metric, defined as

$$\text{MSE}(\hat{\mathbf{H}}) = \mathbb{E} [\|\mathbf{H} - \hat{\mathbf{H}}\|_F^2]. \quad (3)$$

We note that the channel estimation process typically involves denoising the observed pilot measurements, followed by interpolation or extrapolation to infer the channel coefficients at other resource elements in \mathcal{D} .

III. CONVENTIONAL CHANNEL ESTIMATION APPROACHES

In this section, we introduce conventional approaches to the OFDM channel estimation. Existing methods can be broadly categorized into two classes: SP-based approach and DNN-based approach.

A. SP-based Approach

The SP-based OFDM channel estimation strategies have been extensively studied in [6].

Among the various approaches, this work intentionally focuses on pilot-assisted channel estimation, due to its robustness and practicality in wireless communication scenarios. In particular, the LS and MMSE estimators are commonly used as standard methods.

LS: The LS method aims to directly minimize the errors between the received signal and the transmitted pilot signals. Specifically, it seeks to find

$$\hat{\mathbf{H}}_{\text{LS}} = \arg \min_{H[n, m], (n, m) \in \mathcal{P}} \sum_{(n, m) \in \mathcal{P}} |Y[n, m] - H[n, m]X[n, m]|^2, \quad (4)$$

which leads to the following closed-form solution at the pilot positions:

$$\hat{H}[n, m] = \frac{Y[n, m]}{X[n, m]}, \quad (n, m) \in \mathcal{P}. \quad (5)$$

After obtaining the LS estimates at pilot positions, a subsequent interpolation (or extrapolation) step is typically applied to estimate the channel at non-pilot positions $(n, m) \in \mathcal{T} \setminus \mathcal{P}$. Various interpolation techniques can be employed, ranging from simple linear or bilinear interpolation [4], [34].

The LS estimator requires no prior statistical knowledge of the channel or noise, making it simple and straightforward to implement. However, its performance may degrade significantly, especially at low SNR conditions or when the channel matrix \mathbf{H} is ill-conditioned.

MMSE: MMSE estimation uses prior channel statistics to minimize the expected MSE between the true channel and its estimate. It corresponds to the Bayesian conditional mean of the channel given the pilot observations, thus providing a statistically optimal solution to the channel estimation problem. This is given by

$$\hat{\mathbf{H}}_{\text{MMSE}} = \arg \min_{\hat{\mathbf{H}}} \mathbb{E} [\|\mathbf{H} - \hat{\mathbf{H}}\|_F^2 | Y[n, m], (n, m) \in \mathcal{P}] \quad (6)$$

$$= \mathbb{E} [\mathbf{H} | Y[n, m], (n, m) \in \mathcal{P}], \quad (7)$$

where the expectation is taken over the randomness of \mathbf{H} and \mathbf{Z} . Assuming that \mathbf{H} and \mathbf{Z} are jointly Gaussian, the conditional mean (7) is given by the following linear expression:

$$\begin{aligned} \text{vec}(\hat{\mathbf{H}}_{\text{MMSE}}) &= \mathbb{E} [\mathbf{H} | Y[n, m], (n, m) \in \mathcal{P}] \\ &= \mathbf{R}_{\text{vec}(\mathbf{H})\mathbf{H}_p} \mathbf{R}_{\mathbf{Y}_p\mathbf{Y}_p}^{-1} \mathbf{Y}_p, \end{aligned} \quad (8)$$

where $\text{vec}(\mathbf{H}) \in \mathbb{C}^{NM}$ denotes the vectorized full channel matrix, and $\mathbf{H}_p \in \mathbb{C}^L$ represents the vectorized frequency response at the pilot positions. $\mathbf{R}_{\text{vec}(\mathbf{H})\mathbf{H}_p} \in \mathbb{C}^{NM \times L}$ represents the cross-covariance matrix between $\text{vec}(\mathbf{H})$ and \mathbf{H}_p , while $\mathbf{R}_{\mathbf{Y}_p\mathbf{Y}_p} \in \mathbb{C}^{L \times L}$ represents the auto-covariance matrix of \mathbf{Y}_p . More concretely, when \mathbf{Z} is independent and identically distributed Gaussian with variance σ^2 , (8) is further derived as

$$\text{vec}(\hat{\mathbf{H}}_{\text{MMSE}}) = \underbrace{\mathbf{R}_{\text{vec}(\mathbf{H})\mathbf{H}_p} (\mathbf{R}_{\mathbf{H}_p\mathbf{H}_p} + \sigma^2 \mathbf{I})^{-1}}_{\mathbf{W}_{\text{MMSE}} \in \mathbb{C}^{NM \times L}} \mathbf{Y}_p, \quad (9)$$

where \mathbf{W}_{MMSE} indicates the MMSE filter. Accordingly, the estimate corresponding to the specific resource element (n, m) is given by $\hat{H}[n, m] = \mathbf{R}_{H[n, m]\mathbf{H}_p} (\mathbf{R}_{\mathbf{H}_p\mathbf{H}_p} + \sigma^2 \mathbf{I})^{-1} \mathbf{Y}_p$. In this paper, the MMSE refers to the linear MMSE estimator obtained in (8).

Under the joint Gaussian assumption, the MMSE estimator is well-established to achieve optimal MSE performance. Unlike the LS estimator, it exploits knowledge of the covariance matrices $\mathbf{R}_{\text{vec}(\mathbf{H})\mathbf{H}_p}$ and $\mathbf{R}_{\mathbf{H}_p\mathbf{H}_p}$, which enable effective denoising and interpolation by accounting for channel correlations across time and frequency.

Despite its optimality under the Gaussian assumption, the MMSE estimator incurs high computational complexity due to because of the high dimensionality of the covariance matrix in

$\mathbf{R}_{\text{vec}(\mathbf{H})\mathbf{H}_p} \in \mathbb{C}^{NM \times L}$. To address this issue, a low-complexity approximation, termed the 1D frequency-domain MMSE (1D-MMSE) estimator, is proposed. In this method, the temporal-domain channel correlation is neglected, so that only the frequency-domain correlation is taken into account for channel estimation. The 1D-MMSE estimator is given as

$$\hat{\mathbf{H}}_{\text{1D-MMSE}} = \mathbf{R}_{\mathbf{H}[\mathcal{K}]\mathbf{H}[\mathcal{P}]} \left(\mathbf{R}_{\mathbf{H}[\mathcal{P}]\mathbf{H}[\mathcal{P}]} + \sigma^2 \mathbf{I} \right)^{-1} \hat{\mathbf{H}}_{\text{LS}}, \quad (10)$$

where $\mathbf{H}[\mathcal{P}]$ denotes the frequency response at the pilot indices and $\mathbf{H}[\mathcal{K}] \in \mathbb{C}^N$ denotes the full frequency response of all the subcarriers including the pilot component corresponding to $\mathbf{H}[\mathcal{P}]$.

Sensing-aided method: Beyond these purely pilot-based methods, recent research in ISAC has explored sensing-aided extensions that enhance traditional estimators by incorporating auxiliary information. The general framework can be expressed as

$$\hat{\mathbf{H}}_{\text{sensing}} = g(\hat{\mathbf{H}}_{\text{init}}, \theta), \quad (11)$$

where $\hat{\mathbf{H}}_{\text{init}}$ is the initial estimate (e.g., from LS or MMSE) and θ represents auxiliary information from environmental parameters [7] and channel statistics [8]. Enhancement functions include additive refinement ($\hat{\mathbf{H}} = \hat{\mathbf{H}}_{\text{init}} + \Delta\mathbf{H}(\theta)$), multiplication refinement ($\hat{\mathbf{H}} = \mathbf{W}(\theta)\hat{\mathbf{H}}_{\text{init}}$), and projection-based methods. While these approaches can improve estimation accuracy, they require additional sensing infrastructure and computational resources.

Remark 1. Despite their solid theoretical foundations, SP-based methods have several limitations. For instance, MMSE relies on prior knowledge of channel statistics, such as noise variance and channel correlation, which may be difficult to obtain or inaccurate in practical scenarios. Furthermore, MMSE estimation requires matrix inversion, incurring significant computational overhead per channel estimation. While sensing-aided extensions can potentially enhance estimation accuracy by incorporating auxiliary environmental information, they require additional sensing hardware and processing units, which may increase system complexity and cost. Such additional infrastructure could be less suitable for resource-constrained or cost-sensitive applications.

B. DNN-based Approach

To address the limitations of SP-based approaches, DNN-based approaches have been actively explored as a data-driven alternative. The key idea behind existing DNN-based methods is to leverage DNNs as a denoiser and an interpolator for channel estimation. Specifically, by modeling the DNN input as the noisy received pilot signal (i.e., \mathbf{Y}_p) and the output as the corresponding channel estimate (i.e., $\hat{\mathbf{H}}$), we train the DNN to learn a nonlinear mapping between \mathbf{Y}_p and $\hat{\mathbf{H}}$. Existing research on DNN-based approaches can be categorized according to the specific neural network architectures employed for channel estimation.

ChannelNet: ChannelNet [9] represents one of the initial frameworks that exploits a DNN for OFDM channel estimation. In this approach, the channel response is treated

as an image. An initial estimate of the channel is obtained by applying bilinear interpolation to sparsely located pilot symbols, resulting in a low-resolution and noise-contaminated channel map. Then, ChannelNet uses a super-resolution convolutional neural network (i.e., SRCNN) to recover high-resolution spatial features from the interpolated input. After this, a denoising convolutional neural network (i.e., DnCNN) is applied, incorporating residual learning and batch normalization to further refine the estimate.

Channelformer: Channelformer [15] exploits the Attention Transformer architecture for OFDM channel estimation. Unlike ChannelNet, Channelformer flattens the LS channel estimate for all pilot subcarriers into a single vector and feeds its real and imaginary parts as two separate input channels. Based on this, the encoder captures long-range dependencies among sparse pilot embeddings using the Attention Transformer architecture. Instead of the standard Feed-Forward Network, it employs convolutional layers to introduce local inductive bias, while retaining global modeling capabilities through multi-head self-Attention. The decoder refines these context-aware features using a residual convolutional network, integrating both global Attention and local structural information.

For better understanding, we explain the principle of Channelformer as follows. Fundamentally, Channelformer follows the Multi-Head Self-Attention (MHA) mechanism [13]. To be specific, denoting p_i as the complex-valued channel observation at pilot index i with $1 \leq i \leq L$, each pilot observation is first embedded into a two-dimensional real-valued row vector that retains its inherent complex structure: $\mathbf{e}_i = [\Re(p_i), \Im(p_i)] \in \mathbb{R}^2$. Then, we define the full sequence of embedded pilot vectors as

$$\mathbf{X} = [\mathbf{e}_1^\top, \dots, \mathbf{e}_L^\top]^\top \in \mathbb{R}^{L \times 2}, \quad (12)$$

where each row \mathbf{e}_i corresponds to a distinct pilot symbol. This representation serves as the input to the encoder module.

Then, the encoder begins by applying the MHA mechanism to capture local and global dependencies across the sparse pilot positions. Specifically, MHA is computed as:

$$\text{head}_i = \text{Attention}(\mathbf{Q}^{(i)}, \mathbf{K}^{(i)}, \mathbf{V}^{(i)}), \quad i = 1, \dots, h, \quad (13)$$

$$\mathbf{Z} = \text{Concat}(\text{head}_1, \dots, \text{head}_h) \mathbf{W}_O, \quad (14)$$

where the h is equal to 2, representing the number of symbols containing pilots and the Attention operation within each head is the Scaled Dot-Product Attention defined as

$$\text{Attention}(\mathbf{Q}^{(i)}, \mathbf{K}^{(i)}, \mathbf{V}^{(i)}) = \text{softmax} \left(\frac{\mathbf{Q}^{(i)} \mathbf{K}^{(i)\top}}{\sqrt{d_k}} \right) \mathbf{V}^{(i)}. \quad (15)$$

In this formulation, d_k denotes the number of pilot elements within a symbol and each of the query ($\mathbf{Q}^{(i)}$), key ($\mathbf{K}^{(i)}$), and value ($\mathbf{V}^{(i)}$) matrices is obtained by applying linear projections of the input feature vectors as follows:

$$\mathbf{Q}^{(i)} = \mathbf{Z}_{\text{in}} \mathbf{W}_Q^{(i)}, \quad \mathbf{K}^{(i)} = \mathbf{Z}_{\text{in}} \mathbf{W}_K^{(i)}, \quad \mathbf{V}^{(i)} = \mathbf{Z}_{\text{in}} \mathbf{W}_V^{(i)}, \quad (16)$$

where \mathbf{Z}_{in} denotes the input feature matrix. $\mathbf{W}_Q^{(i)}$, $\mathbf{W}_K^{(i)}$, and $\mathbf{W}_V^{(i)}$ are learnable weight matrices corresponding to the i^{th}

head. Additionally, \mathbf{W}_O denotes a weight matrix used for merging information across all heads.

Unlike the conventional Attention Transformer encoder that employs a position-wise Feed-Forward Network (FFN) following MHA, Channelformer introduces a convolutional layer to enhance local spatial modeling:

$$\mathbf{Z}' = \text{Conv}(\mathbf{Z}), \quad \mathbf{H}_{\text{enc}} = \text{Norm}(\mathbf{Z} + \mathbf{Z}'), \quad (17)$$

where \mathbf{H}_{enc} represents the final encoder output, enriched with both global and local contextual information. The rationale behind incorporating convolutional layers is to inject local inductive biases into the global Attention-based features, enabling the network to capture intricate local channel variations effectively.

The decoder maps the encoded representations to the full channel estimate through a residual convolutional neural network ($\mathcal{F}_{\text{ResCNN}}(\cdot)$):

$$\hat{\mathbf{H}} = \mathcal{F}_{\text{ResCNN}}(\mathbf{H}_{\text{enc}} | \theta_{\text{dec}}), \quad \hat{\mathbf{H}} \in \mathbb{C}^{N \times M}, \quad (18)$$

where θ_{dec} denotes the learnable parameters of the decoder.

Remark 2. DNN-based channel estimation approaches have several benefits. Notably, they do not require direct prior knowledge of channel statistics, which enhances their practical applicability. Additionally, the powerful learning capabilities of DNNs are able to capture the channel's correlation structures directly from training data, facilitating accurate channel estimation even in challenging scenarios such as high-mobility environments. Nonetheless, these approaches are limited by: i) a large number of model parameters and nonlinear computations, and ii) a lack of flexibility in easily adjusting the computational overhead according to the user's computation capability. We note that these shortcomings mainly arise because existing DNN-based architectures (including SRCNN and Attention Transformer) are directly used to produce channel estimation outputs. As a result, several nonlinear activation functions are unavoidable, and the number of model parameters is difficult to control.

IV. ATTENTION-AIDED MMSE

In this section, we propose the A-MMSE method for OFDM channel estimation. Our key idea is to learn linear estimation filter coefficients using the Attention Transformer rather than directly employing a DNN to produce channel estimates. Once trained, the learned filters are applied to noisy pilot signals to yield channel estimates through a linear operation, resembling the structure of the classical SP-based MMSE estimation approach. In the following, we present a detailed explanation of the proposed A-MMSE method. For clarity of exposition, we first describe the A-MMSE estimation mechanism, followed by the A-MMSE learning mechanism.

A. A-MMSE Estimation Mechanism

In the proposed A-MMSE approach, channel estimation follows conventional linear processing. Specifically, the estimated channel matrix $\hat{\mathbf{H}}_{\text{A-MMSE}}$ is obtained by

$$\text{vec}(\hat{\mathbf{H}}_{\text{A-MMSE}}) = \mathbf{W}_{\text{A-MMSE}} \mathbf{Y}_p, \quad (19)$$

where $\mathbf{W}_{\text{A-MMSE}}$ represents the A-MMSE linear filter. The A-MMSE filter $\mathbf{W}_{\text{A-MMSE}}$ is learned through our Attention Transformer architecture as follow:

$$\mathbf{W}_{\text{A-MMSE}} = \mathcal{F}_{\text{A-MMSE}}([\mathfrak{R}(Y[n, m]); \mathfrak{I}(Y[n, m])], \\ (n, m) \in \mathcal{P} | \theta_{\text{A-MMSE}}) \quad (20)$$

where $\mathcal{F}_{\text{A-MMSE}}(\cdot)$ represents the Attention Transformer network and $\theta_{\text{A-MMSE}}$ denotes learnable parameters of A-MMSE.

Remark 3. It is important to highlight several key points regarding the proposed A-MMSE method. First, by leveraging the Attention Transformer to learn $\mathbf{W}_{\text{A-MMSE}}$, A-MMSE inherits the primary advantages of DNN-based approaches: powerful learning capability and no requirement for prior channel statistics. Second, once $\mathbf{W}_{\text{A-MMSE}}$ is learned, we only use linear computation as presented in (19), avoiding the computational complexity associated with nonlinear activation functions in the channel estimation process. In this sense, the proposed A-MMSE is a hybrid approach that effectively combines SP-based and DNN-based approaches. Further, in the A-MMSE framework, it is possible to adjust the number of effective parameters within $\mathbf{W}_{\text{A-MMSE}}$, so that the A-MMSE adapts its computational overheads depending on various environments. We further explore this in the next section.

B. A-MMSE Learning Mechanism

1) *Insights on Two-Stage Attention Encoder:* We now provide a detailed explanation of the A-MMSE learning mechanism $\mathcal{F}_{\text{A-MMSE}}(\cdot)$ (20), whose overall architecture and training pipeline are depicted in Fig. 2. Structurally inspired by recent encoder-decoder architectures based on Attention Transformer, the proposed A-MMSE method incorporates theoretical insights derived from classical SP-based channel estimation approaches. Specifically, as shown in the MMSE filter structure (9), the optimal linear filter operates by first whitening the pilot observations and then interpolating the full OFDM channel using the underlying frequency-temporal domain channel correlation. This highlights the importance of explicitly incorporating the channel's second-order statistics. The proposed A-MMSE learning mechanism effectively captures the correlation structure inherent to OFDM channels. Its detailed formulation is presented as follows.

Under the assumption of a wide-sense stationary uncorrelated scattering (WSSUS) environment and separable scattering function [35], the second-order statistics of OFDM channels exhibit a separable correlation function across frequency and temporal domains. Formally, the channel correlation matrix between two channel taps separated by frequency index difference Δn and time index difference Δm is factorized as follows:

$$\mathbf{R}_h(\Delta n, \Delta m) = \mathbb{E}[\mathbf{H}[n, m] \mathbf{H}^*[n + \Delta n, m + \Delta m]] \\ = r_f(\Delta n) \cdot r_t(\Delta m), \quad (21)$$

where $r_f(\Delta n)$ and $r_t(\Delta m)$ represent the frequency-domain and temporal-domain correlation, respectively. Upon discretizing this correlation (21) over the OFDM grid, the covariance matrix of the OFDM channel is given by

$$\mathbf{R}_{\text{full}} = \mathbb{E}[\mathbf{h}\mathbf{h}^H] \approx \mathbf{R}_f \otimes \mathbf{R}_t \in \mathbb{C}^{NM \times NM}, \quad (22)$$

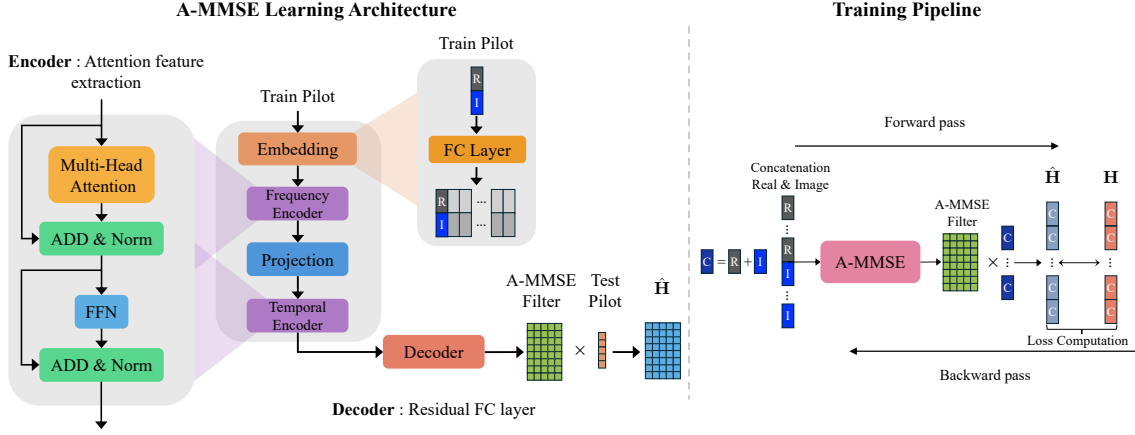


Fig. 2. Architecture and end-to-end training pipeline of the proposed A-MMSE network for learning the MMSE filter

where \mathbf{h} denotes $\text{vec}(\mathbf{H}) \in \mathbb{C}^{NM}$, $\mathbf{R}_f \in \mathbb{C}^{N \times N}$ and $\mathbf{R}_t \in \mathbb{C}^{M \times M}$ represent the frequency and temporal domain correlation matrices, respectively, as visualized in Fig. 3. A detailed proof of this Kronecker product structure is provided in Appendix A. We note that the approximation (\approx) in (22) arises because the WSSUS assumption may not perfectly hold in practical scenarios. The representation of the full covariance matrix \mathbf{R}_{full} as the Kronecker product (\otimes) between the frequency-domain correlation \mathbf{R}_f and the temporal-domain correlation \mathbf{R}_t (22) implies that the frequency-temporal domain correlation structure is separable. This allows for a compact and computationally efficient representation of the channel covariance matrix. Building on this insight, we propose the following two-stage encoder design.

- **Frequency Encoder:** In the Frequency Encoder stage, the pilot observations are processed along the subcarrier domain, extracting features on the frequency-domain correlation structure at pilot indices, corresponding to row of the matrix $\mathbf{R}_f[\mathcal{P}, :]$.
- **Temporal Encoder:** In the Temporal Encoder stage, the output of the Frequency Encoder is then subsequently processed along the OFDM symbol domain, capturing temporal-domain correlation structures at pilot indices, corresponding to rows of the matrix $\mathbf{R}_t[\mathcal{P}, :]$.

This two-stage encoder enables the model to learn the joint frequency–temporal correlation structure; each stage uses a single encoder block, which is critical for the accurate MMSE estimation. Crucially, we note that this encoder design represents a key distinction of the proposed A-MMSE learning mechanism compared to conventional DNN-based methods. Specifically, existing approaches typically adopt standard learning architectures such as CNN [9] or Attention Transformer [15], without explicitly tailoring them to the statistical properties inherent in OFDM channels. In contrast, our method explicitly incorporates the inherent temporal and frequency-domain correlation structures of OFDM channels into the learning process. This integration not only enhances learning efficiency but also improves the model’s capability to generalize under practical channel conditions. In this sense, the proposed A-MMSE approach is distinguished not only by

its design, which enables the learning of a linear estimation filter rather than directly estimating the OFDM channel matrix (as illustrated in Fig.1), but also by its advanced learning mechanism that explicitly reflects the inherent correlation structure of OFDM channels.

2) *Multi-Head Self-Attention Mechanism:* Building upon the proposed two-stage encoder structure, we use the MHA mechanism in (13)–(16) to extract encoded features. In particular, the Frequency Encoder captures correlations between pilot observations and individual subcarriers, thus its number of attention heads is fixed to the pilot count within a single OFDM symbol. The Temporal Encoder then extends the resulting frequency-domain features along the symbol axis to model the inter-symbol correlation. Accordingly, the number of attention heads is set equal to the total number of OFDM symbols considered. The statistical features extracted by the two-stage encoder are subsequently passed through a residual fully connected decoder, which maps them into the coefficient space of the A-MMSE filter. The detailed process is as follows.

Frequency Encoder: The detailed structure of the two-stage encoder is depicted in Fig. 3. In the first stage, a linear embedding layer transforms the raw pilot input data into a high-dimensional embedding space, where the embedding dimension matches the number of subcarriers. This embedding is essential to facilitate the subsequent MHA mechanism, which effectively captures the frequency-domain dependencies inherent among the pilot signals. Specifically, the noisy pilot vector is given by $\mathbf{x}_{\text{in}} = [x_1, x_2, \dots, x_{2L}]^T \in \mathbb{R}^{2L}$. Here, each scalar x_i is linearly embedded into a high-dimensional vector as: $\mathbf{x}_{\text{emb},i} = x_i \cdot \mathbf{P}_{\text{emb}} + \mathbf{b}_{\text{emb}}$, where $\mathbf{P}_{\text{emb}} \in \mathbb{R}^{1 \times d_e}$ is a learnable projection matrix and $\mathbf{b}_{\text{emb}} \in \mathbb{R}^{d_e}$ is a learnable bias vector. Stacking all $\mathbf{x}_{\text{emb},i}$, we have

$$\mathbf{X}_{\text{Emb}} = [\mathbf{x}_{\text{emb},1}^T, \mathbf{x}_{\text{emb},2}^T, \dots, \mathbf{x}_{\text{emb},2L}^T]^T \in \mathbb{R}^{2L \times d_e}. \quad (23)$$

The embedding dimension d_e is set equal to N (the number of subcarriers), ensuring that the resulting embedded representations effectively capture complex frequency-domain characteristics.

Subsequently, the embedding matrix \mathbf{X}_{Emb} is fed into the MHA module ($\mathcal{F}_{\text{MHA}}(\cdot)$) with the number of heads fixed at L

, where L equals the total number of DM-RS pilot symbol (one head per pilot). Each complete pilot is split into real and imaginary parts, resulting in the $2L$ column dimension of \mathbf{X}_{Emb} . For example, with Type-A DM-RS and additional Position = 1 (i.e., two DM-RS OFDM symbols) using a comb-2 pattern over 6 resource blocks (RBs), that has 72 subcarriers, there are $72/2 = 36$ pilots per DM-RS symbol, hence $L = 36 \times 2 = 72$ pilots in total. In general,

$$L = \left(\frac{N_{\text{RB}} \cdot N_{\text{SC/RB}}}{2} \right) \times N_{\text{DM-RS sym}}, \quad (24)$$

where N_{RB} is the number of resource blocks, $N_{\text{SC/RB}} = 12$ is the number of subcarriers per RB, and $N_{\text{DM-RS sym}}$ denotes the number of OFDM symbols carrying DM-RS. The operation of the MHA module $\mathcal{F}_{\text{MHA}}(\cdot)$ is described in (13)–(16). We note that this allows each head to learn distinct frequency domain correlation patterns. Following the MHA module, Add & Layer Normalization is applied, succeeded by a FFN, and subsequently another Add & Layer Normalization, in sequential order. Details on Add & Norm and FFN are provided in [13]. After these processes, the encoder extracts frequency-domain statistical information, which can be formally represented as

$$\mathbf{Y}_{\text{Freq}} = \mathcal{E}_{\text{Frequency}} (\mathcal{F}_{\text{MHA}}(\mathbf{X}_{\text{Emb}} | \theta_{\text{MHA, Freq}}) | \theta_{\text{Freq}}) \quad (25)$$

where $\mathbf{Y}_{\text{Freq}} \in \mathbb{R}^{2L \times N}$ represents features encoded by the Frequency Encoder, $\mathcal{E}_{\text{Frequency}}$ represents the Frequency Encoder module, and $\theta_{\text{MHA, Freq}}$ and θ_{Freq} denote the learnable parameters of MHA module and the combined parameters of the two Add & Layer Normalization and FFN, respectively. Correspondingly, the overall operation $\mathbf{x}_{\text{in}} \mapsto \mathbf{Y}_{\text{Freq}}$ yields a real-valued matrix, where each row corresponds to a pilot position and columns aligns with subcarrier-specific embedding dimensions, explicitly capturing both local and global dependencies in the frequency domain.

Temporal Encoder: In the second stage, a linear projection layer transforms the features encoded in the previous stage into a high dimensional frequency-temporal domain, where the projection dimension is NM . The encoded feature matrix is given as $\mathbf{Y}_{\text{Freq}} = [\mathbf{y}_{\text{freq},1}; \mathbf{y}_{\text{freq},2}; \dots; \mathbf{y}_{\text{freq},2L}] \in \mathbb{R}^{2L \times N}$. Here, each row vector $\mathbf{y}_{\text{freq},i}$ is linearly projected as $\mathbf{x}_{\text{proj},i} = \mathbf{y}_{\text{freq},i} \cdot \mathbf{P}_{\text{proj}} + \mathbf{b}_{\text{proj}}$, where $\mathbf{P}_{\text{proj}} \in \mathbb{R}^{N \times d_p}$ is a learnable projection matrix and $\mathbf{b}_{\text{proj}} \in \mathbb{R}^{d_p}$ is a learnable bias vector. Stacking all projected vectors $\mathbf{x}_{\text{proj},i}$, this yields the matrix given by

$$\mathbf{X}_{\text{Proj}} = [\mathbf{x}_{\text{proj},1}^T; \mathbf{x}_{\text{proj},2}^T; \dots; \mathbf{x}_{\text{proj},2L}^T]^T \in \mathbb{R}^{2L \times d_p}. \quad (26)$$

We note that the projection dimension d_p is set to NM , ensuring that the model captures the frequency-temporal correlation of the OFDM channel, as formulated in (22).

Next, the projected matrix \mathbf{X}_{Proj} is fed into another MHA module, with the number of heads fixed at M (one head for each OFDM symbol). Similar to the above, this enables each to effectively learn distinct temporal correlation patterns. The subsequent process is identical to that of the Frequency Encoder.

After completing all the steps, the frequency-temporal statistical information extracted by the Temporal Encoder can be represented as follows:

$$\mathbf{Y}_{\text{Temp}} = \mathcal{E}_{\text{Temporal}} (\mathcal{F}_{\text{MHA}}(\mathbf{X}_{\text{Proj}} | \theta_{\text{MHA, Temp}}) | \theta_{\text{Temp}}) \quad (27)$$

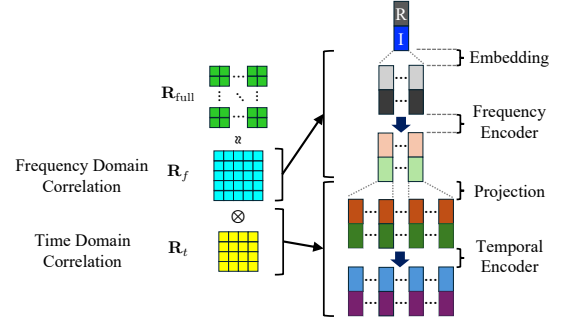


Fig. 3. Detailed structure of the proposed two-stage Attention encoder.

where $\mathbf{Y}_{\text{Temp}} \in \mathbb{R}^{2L \times NM}$ represents features encoded by the Temporal Encoder, $\mathcal{E}_{\text{Temporal}}$ represents the Temporal Encoder module, with $\theta_{\text{MHA, Temp}}$ and θ_{Temp} being the learnable parameters of MHA module and the combined parameters of the two Add & Layer Normalization and FFN, respectively. The overall operations $\mathbf{Y}_{\text{Freq}} \mapsto \mathbf{Y}_{\text{Temp}}$ yield a real-valued matrix, whose rows correspond to pilot positions and whose columns align with subcarrier-symbol specific embedding dimensions. This explicitly captures both local and global dependencies in the frequency-temporal domain of the OFDM channel. The frequency-temporal features encoded by the two-stage encoder serve as inputs to the decoder.

Residual Fully Connected Decoder: Now we describe the decoder structure. The decoder of the A-MMSE model employs a residual fully connected (ResFC) module. Through this, we aim to reconstruct the final A-MMSE filter, from the encoded frequency-temporal features.

The decoder input, i.e., \mathbf{Y}_{Temp} , is processed through multiple fully connected layers with residual connections to ensure stable training and efficient transformation. The output dimension of the decoder remains consistent with its input dimension. This is presented as

$$\mathbf{Y}_{\text{Dec}} = \mathcal{F}_{\text{ResFC}} (\mathbf{Y}_{\text{Temp}} | \theta_{\text{ResFC}}) \in \mathbb{R}^{2L \times NM}, \quad (28)$$

where $\mathbf{Y}_{\text{Dec}} \in \mathbb{R}^{2L \times NM}$ represents the A-MMSE filter coefficients mapped by the ResFC decoder, and θ_{ResFC} denotes the learnable decoder parameters.

Once \mathbf{Y}_{Temp} is obtained, it is partitioned into the real and imaginary components as follows.

$$\mathbf{W}_{\text{real}} = \mathbf{Y}_{\text{Dec}}[1 : L, :] \in \mathbb{R}^{L \times NM}, \quad (29)$$

$$\mathbf{W}_{\text{imag}} = \mathbf{Y}_{\text{Dec}}[L + 1 : 2L, :] \in \mathbb{R}^{L \times NM}. \quad (30)$$

Then, the final complex-valued filter matrix is reconstructed by combining these two components as

$$\mathbf{W}_{\text{out}} = \mathbf{W}_{\text{real}} + j \mathbf{W}_{\text{imag}}, \quad \mathbf{W}_{\text{A-MMSE}} = \mathbf{W}_{\text{out}}^T \in \mathbb{C}^{NM \times L}. \quad (31)$$

This completes the end-to-end A-MMSE learning pipeline.

3) *Training Method:* The proposed A-MMSE model is trained in an end-to-end fashion as shown in the training pipeline of Fig. 2. The model parameters are optimized by minimizing a certain loss function, which quantifies the dis-

crepancy between the estimated and true channel responses across the entire dataset:

$$\text{Loss} = \frac{1}{N_{\mathcal{B}} \times \mathcal{B}} \sum_{j=1}^{N_{\mathcal{B}}} \sum_{i=1}^{\mathcal{B}} \mathcal{L}(\hat{\mathbf{H}}_{i,j}, \mathbf{H}_{i,j}), \quad (32)$$

where $N_{\mathcal{B}}$ denotes the number of mini batch and \mathcal{B} denotes the mini batch size. In addition, $\mathbf{H}_{i,j}$ and $\hat{\mathbf{H}}_{i,j}$ represent the corresponding true channel matrix and estimated channel matrix, respectively. For the loss function $\mathcal{L}(\cdot)$, MSE or Huber loss can be chosen. We discuss this further in the next subsection. The loss function (32) is minimized via backpropagation and the Adam optimizer [36].

After training, one final A-MMSE filter is produced from the entire training dataset. This A-MMSE filter remains fixed and is consistently applied to all test data without further modification.

C. Discussions

Now we provide further insights regarding the proposed A-MMSE method.

1) *MSE and Huber Loss*: Possible choices for the loss function $\mathcal{L}(\cdot)$ include MSE and Huber loss [37]. We explain these as follows.

- **MSE**: For simplicity, we omit the mini batch index j from (32). For a mini-batch of size \mathcal{B} , the MSE is defined as

$$\text{MSE} = \frac{1}{\mathcal{B}} \sum_{i=1}^{\mathcal{B}} \|\hat{\mathbf{H}}_i - \mathbf{H}_i\|_F^2,$$

with its gradient derived as $\nabla_{\hat{\mathbf{H}}_i} \text{MSE} = 2(\hat{\mathbf{H}}_i - \mathbf{H}_i)$. The loss is convex and smooth, facilitating straightforward optimization. However, its quadratic growth makes the loss sensitive to outliers, as a single large residual can dominate the objective, undermining robustness.

- **Huber Loss**: With residual $a_i = \hat{\mathbf{H}}_i - \mathbf{H}_i$ and transition threshold $\delta > 0$, Huber loss is defined as

$$L_{\delta}(a_i) = \begin{cases} \frac{1}{2}a_i^2, & |a_i| \leq \delta, \\ \delta\left(|a_i| - \frac{1}{2}\delta\right), & |a_i| > \delta, \end{cases}$$

with its gradient

$$\nabla_{\hat{\mathbf{H}}_i} L_{\delta}(a_i) = \begin{cases} a_i, & |a_i| \leq \delta, \\ \delta \text{sgn}(a_i), & |a_i| > \delta. \end{cases}$$

The loss function is quadratic near the origin and linear in the tails, limiting the influence of each outlier at $\mathcal{O}(\delta)$. In practice, δ can be chosen inversely proportional to the operating SNR, e.g., higher SNR implies cleaner observations and thus a smaller δ , whereas lower SNR favors a larger δ to mitigate noise-induced outliers.

To improve robustness to noise and extreme outliers, and better reflect channel statistics, we train A-MMSE with the Huber loss, which stabilizes learning. As demonstrated in Fig. 4, Huber loss consistently outperform MSE loss, particularly at high SNR where its bounded gradient prevents occasional large residuals from destabilizing the training process—achieving up to 17% lower NMSE at 30 dB SNR. The detailed training methodology using Huber loss and its implementation for channel estimation are explained in Section VI.

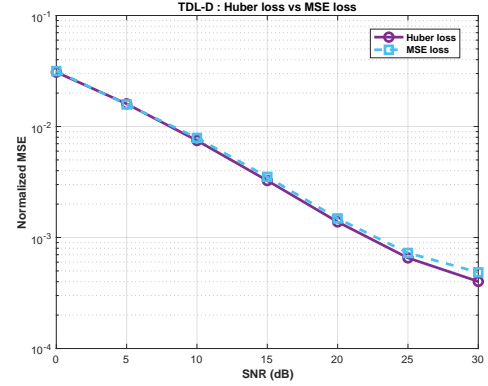


Fig. 4. 5G NR time-frequency resource block with Type A DM-RS.

2) *Complexity*: The proposed A-MMSE is fundamentally distinguished from existing DNN-based channel estimation approaches. To be specific, the proposed A-MMSE method learns a linear filter matrix $\mathbf{W}_{\text{A-MMSE}}$ during a dedicated training phase. As a result, once trained, channel estimation reduces to a single matrix-vector multiplication, as shown in (19). This enables highly efficient inference, with minimal computational cost and requiring only $2(NM \times L)$ real-valued parameters to store $\mathbf{W}_{\text{A-MMSE}}$. In contrast, as discussed earlier, conventional DNN-based methods [9], [15] learn a neural network that maps pilot inputs directly to channel outputs. As a result, each inference (i.e., channel estimation) involves propagating the input through multiple layers of nonlinear operations, leading to higher inference complexity. Specifically, the A-MMSE performs channel estimation using only linear operations with approximately 70,000 ($= NM \times L$) parameters, whereas Channelformer requires about 110,000 parameters and includes nonlinear components, such as GELU activations and convolutional layers.

Nevertheless, the A-MMSE may still face challenges related to computational complexity and memory constraints especially as N, M or L increase. For example, despite its linear structure, storing the full matrix $\mathbf{W}_{\text{A-MMSE}}$ and performing large-scale matrix-vector multiplications can still be burdensome, particularly for users with limited computational resources. Hence, it is desirable to adapt the computation and memory requirements of A-MMSE depending on the available system resources. To this end, we propose a new technique that dynamically adjusts the filter structure, as detailed in the following section.

V. RANK-ADAPTIVE A-MMSE

In this section, by extending the A-MMSE, we introduce the RA-A-MMSE framework, whose architecture is illustrated in Fig. 5. The RA-A-MMSE incorporates a rank-adaptation (RA) mechanism that adaptively reduces the filter matrix rank according to resource constraints, such as a predefined maximum rank (r) or a limit on the number of filter parameters. By flexibly adjusting the rank to satisfy these constraints, the RA-A-MMSE effectively reduces computational and memory overhead, allowing the filter to operate efficiently even under stringent computation resource limitations. Despite operating at a reduced rank, the RA-A-MMSE still maintains high

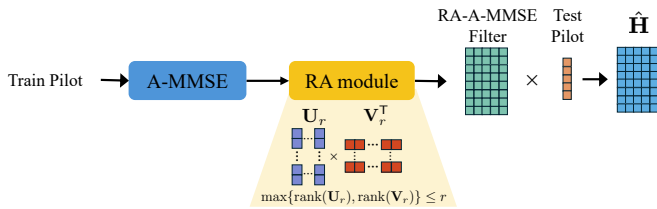


Fig. 5. RA-A-MMSE architecture: a rank-adaptation module is appended to A-MMSE to flexibly adjust the rank of the learned A-MMSE filter.

estimation accuracy. It thus offers a practical and scalable solution for resource-constrained OFDM receivers, achieving a favorable balance between performance and hardware efficiency.

To explain the key idea of RA-A-MMSE, we begin by examining how rank reduction alleviates computational complexity. Recall that the A-MMSE filter $\mathbf{W}_{\text{A-MMSE}} \in \mathbb{C}^{NM \times L}$ is a linear transformation from the pilot observations to the channel estimate. Accordingly, without any rank-specific modification, the A-MMSE channel estimation requires linear operations proportional to $8NM \times L$, accounting for both real and imaginary components in complex-valued multiplications. Now suppose that the rank of $\mathbf{W}_{\text{RA-A-MMSE}}$ is reduced to r . Then the following rank- r factorization is allowed:

$$\mathbf{W}_{\text{RA-A-MMSE}} \approx \mathbf{A}\mathbf{B}^T, \quad \mathbf{A} \in \mathbb{C}^{NM \times r}, \mathbf{B} \in \mathbb{C}^{L \times r}. \quad (33)$$

In this case, the estimation process can be decomposed into two sequential steps:

$$\tilde{\mathbf{Y}}_p = \mathbf{B}^T \mathbf{Y}_p, \quad \text{vec}(\hat{\mathbf{H}}_{\text{RA-A-MMSE}}) = \mathbf{A} \tilde{\mathbf{Y}}_p, \quad (34)$$

where $\mathbf{Y}_p \in \mathbb{C}^L$ is the pilot input and $\text{vec}(\hat{\mathbf{H}}_{\text{RA-A-MMSE}})$ is the channel estimate. This decomposition reduces the computational complexity to approximately $8rL + 8NM r$ real-valued operations, which is significantly lower than the full-rank case when $r \ll \min(NM, L)$.

To achieve the rank reduction in the RA-A-MMSE, we devise a rank-adaptive (RA) module that produces two trainable matrices, $\mathbf{U}_r \in \mathbb{R}^{NM \times r}$ and $\mathbf{V}_r \in \mathbb{R}^{L \times r}$, where r denote the desired rank. With \mathbf{U}_r and \mathbf{V}_r , the A-MMSE filter matrix $\mathbf{W}_{\text{A-MMSE}}$ is modified to $\mathbf{W}_{\text{RA-A-MMSE}} = \mathbf{W}_{\text{A-MMSE}} \mathbf{U}_r \mathbf{V}_r^T$. Then the rank of $\mathbf{W}_{\text{RA-A-MMSE}}$ is bounded by

$$\text{rank}(\mathbf{W}_{\text{A-MMSE}} \mathbf{U}_r \mathbf{V}_r^T) \leq \min\{\text{rank}(\mathbf{W}_{\text{A-MMSE}}), \text{rank}(\mathbf{U}_r), \text{rank}(\mathbf{V}_r)\} \leq r, \quad (35)$$

where the last inequality holds if $r \leq \min\{NM, L\}$. As a result, the rank of $\mathbf{W}_{\text{RA-A-MMSE}}$ is bounded by r , allowing the effective filter rank to be adaptively controlled via the

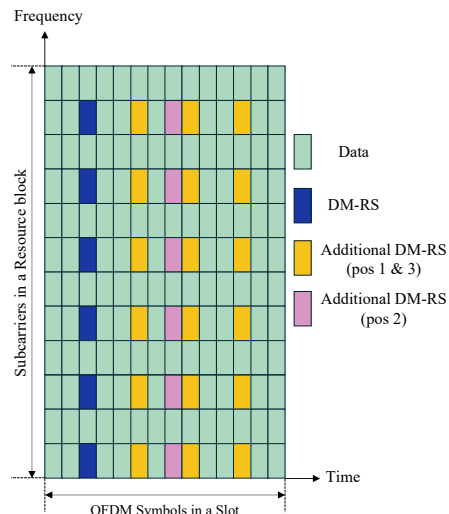


Fig. 6. 5G NR time-frequency resource block with Type A DM-RS.

dimensions of \mathbf{U}_r and \mathbf{V}_r . This enables the RA-A-MMSE to flexibly adapt to available system resources.

Compared to the A-MMSE, the computational cost reduction of the RA-A-MMSE can be quantified by the ratio

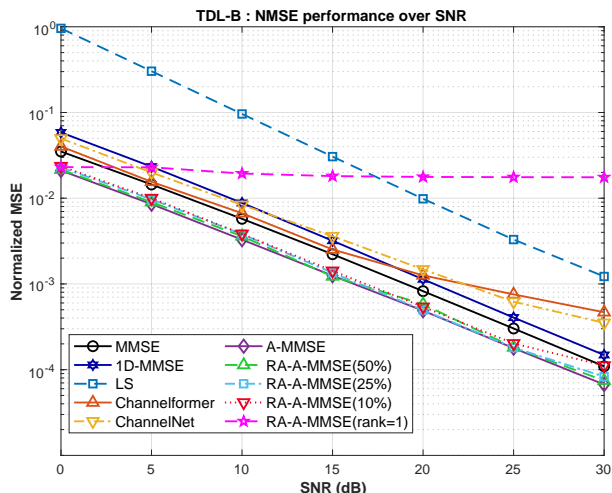
$$\text{Complexity Cost Ratio: } \frac{\text{RA-A-MMSE}}{\text{A-MMSE}} \approx \frac{NM r + L r}{NML} \quad (36)$$

Considering an OFDM channel comprising 6 RBs (minimum bandwidth assignment), i.e., $N = 72$, $M = 14$, and $L = 36$ or 72 , the RA-A-MMSE with $r = 12$ has the reduced computational cost by approximately 35% and 18% for $L = 36$ and $L = 72$, respectively. Moreover, since the RA module leverages learnable matrices (\mathbf{U}_r and \mathbf{V}_r) optimized during training, this substantial complexity reduction can be achieved with minimal channel estimation performance loss. We demonstrate this in the next section.

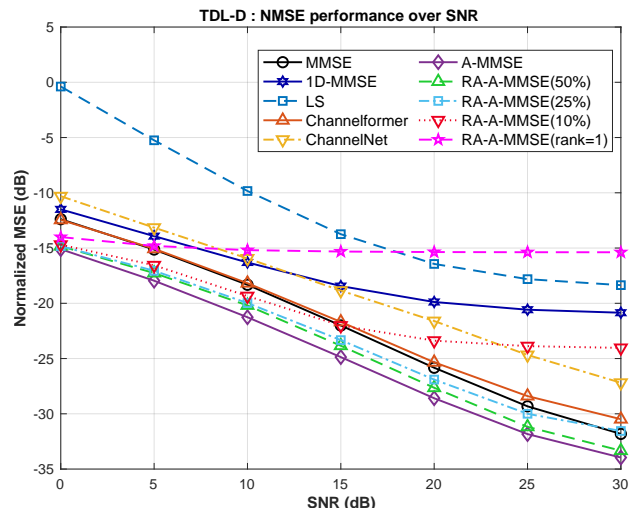
Remark 4. The proposed A-MMSE method exploits sparsity in two primary ways. First, the two-stage Attention encoder implicitly leverages sparsity through its MHA mechanism, which naturally induces soft-sparsity by assigning higher weights to dominant features while suppressing less significant ones. This aligns well with wideband wireless channels that can be captured by a separable, low-rank covariance model ($\mathbf{R}_{\text{full}} \approx \mathbf{R}_f \otimes \mathbf{R}_t$). Second, the Rank-Adaptive A-MMSE (RA-A-MMSE) framework exploits the rank-deficient structure inherent in the ideal MMSE filter, where all rows share a common whitening filter and differ only by position-dependent correlation coefficients. By learning to identify and operate within this naturally sparse subspace, RA-A-MMSE achieves

TABLE I
TDL CHANNEL SPECIFICATION

	Scenario	Carrier Freq. [Hz]	Delay Spread [ns]	SCS [Hz]	Velocity [km/h]	Max Doppler [Hz]	Propagation
TDL-A	Indoor office	2G	30	15K	5	9.26	NLOS
TDL-B	UMi Street-canyon	3.5G	100	30K	30	97.2	NLOS
TDL-C	UMa	3.5G	300	30K	100	324.1	NLOS
TDL-D	RMa O2I	5G	300	60K	300	1388.9	LOS+NLOS
TDL-E	UMa O2I	28G	1000	120K	120	3111.1	LOS+NLOS



(a) NMSE performance under the TDL-B Scenario (UMi Street-canyon)



(b) NMSE performance under the TDL-D Scenario (RMa O2I)

Fig. 7. NMSE comparison over SNR: (a) TDL-B and (b) TDL-D scenarios.

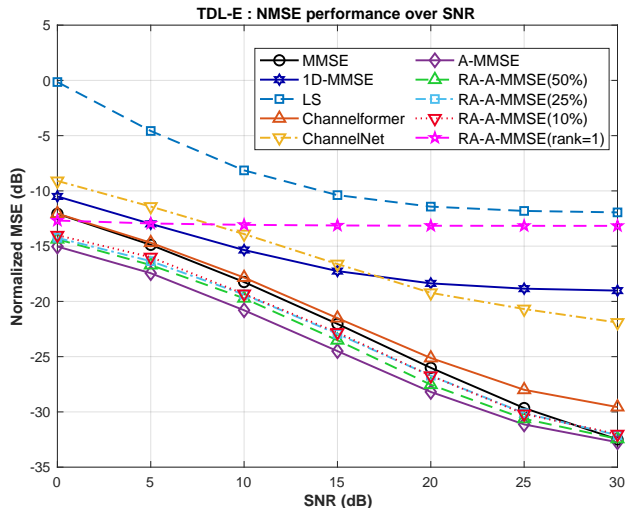


Fig. 8. NMSE comparison over SNR: TDL-E scenario.

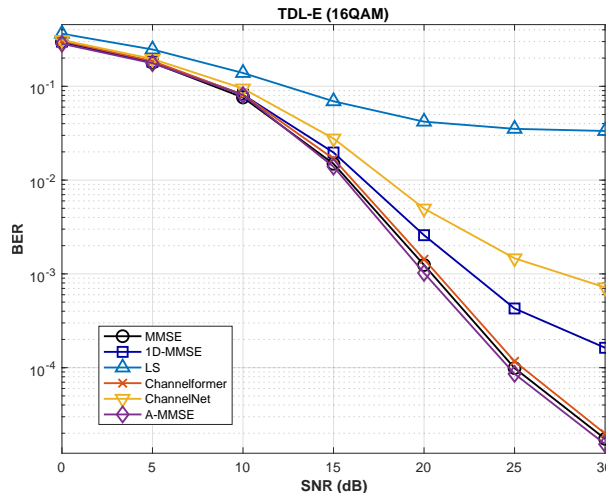


Fig. 9. BER performance under 16-QAM modulation for the 3GPP TDL-E channel model.

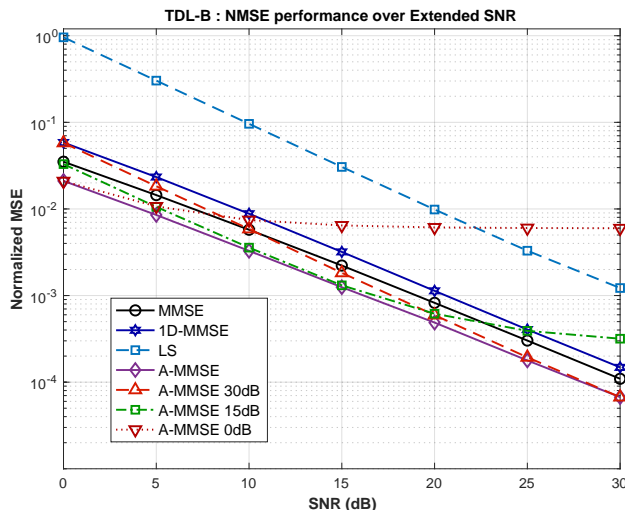
dramatic rank reduction without significant performance loss. As shown in Section VI, RA-A-MMSE maintains 99.6% of its performance with only 10% of the full rank, demonstrating that it identifies the naturally sparse subspace where MMSE channel estimation resides rather than simply discarding information.

VI. SIMULATION RESULTS

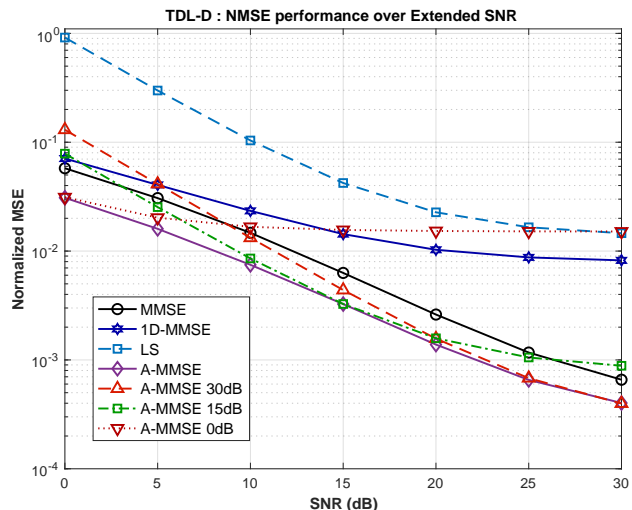
A. Simulation Setup

For numerical simulations, we follow the 5G NR DM-RS configuration from 3GPP TS 38.211 [38]. DM-RS's time-frequency density adapts to channel conditions: front-loaded configurations suit slowly varying channels, while rapidly varying channels require additional symbols to track the dynamics. Frequency selectivity further affects DM-RS pattern design, requiring a trade-off between estimation accuracy and pilot overhead. We illustrate this in Fig. 6.

We evaluate channel estimation performance using TDL channel models (TDL-A to TDL-E) specified in 3GPP TR 38.901, which capture realistic multipath propagation scenarios (see Table I). For each scenario, a continuous sequence of 44,000 OFDM frames was generated using a standard channel model simulator. By running the channel model continuously without resets and dynamically updating the Doppler shift to model user mobility, we intentionally created a non-stationary channel where the WSSUS assumption is broken globally and holds only locally over short intervals. The generated dataset was partitioned to test generalization: the last 4,000 frames served as the test set with temporal separation from the initial 40,000 frames, which were divided into 36,000 training frames and 4,000 validation frames. This temporal split ensures natural statistical drift between training and test sets, providing a realistic measure of robustness. Model training was conducted using TensorFlow on a single NVIDIA

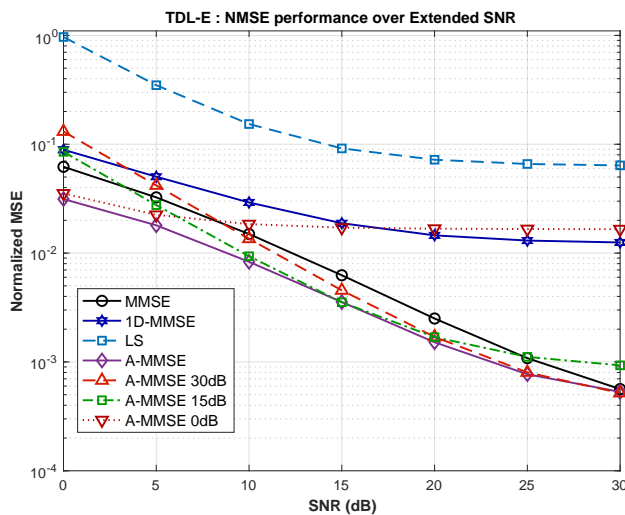


(a) NMSE performance under the TDL-B Scenario (UMi Street-canyon) over extended SNR

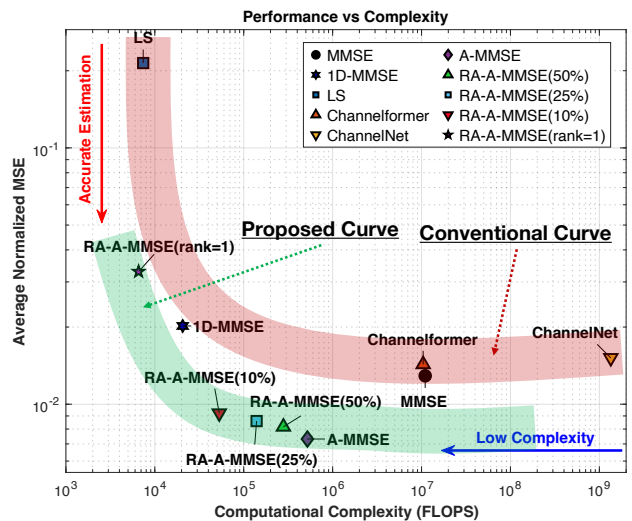


(b) NMSE performance under the TDL-D Scenario (RMa O2I) over extended SNR

Fig. 10. NMSE performance comparison of various channel estimation methods over extended SNR under (a) TDL-B and (b) TDL-D channel scenarios.



(a) NMSE Performance over extended SNR for TDL-E Scenario (mmWave)



(b) Average NMSE vs. Computational Complexity (FLOPs) over all channels, comparing the proposed and conventional estimation curves

Fig. 11. NMSE performance over extended SNR (left) and NMSE-complexity trade-off across channels (right) for the proposed and conventional estimators.

GeForce RTX 4090 GPU.

Due to space limitations, we focus on three representative TDL models: TDL-B (typical urban), TDL-D (high mobility), and TDL-E (mmWave), which together span a broad range of deployment scenarios across frequency bands. The diverse subcarrier spacings specified in Table I, corresponding to different symbol durations, are chosen intentionally to evaluate the proposed method across the fundamental trade-off between Doppler resolution and robustness to channel time-variations. As benchmark methods, we consider the following. For SP-based approaches, we include LS, MMSE, and 1D-MMSE. For DNN-based approaches, we include ChannelNet [9] and Channelformer [15]. Furthermore, in the final subsection, we also compare the performance of a sensing-aided approach [7] and A-MMSE.

B. On the Suboptimality of Covariance-Mismatched MMSE Estimation

As described in subsection VI-A, our dataset was intentionally generated to break the WSSUS assumption globally, creating a non-stationary environment where channel statistics vary across OFDM frames. This directly causes covariance mismatch in conventional MMSE estimation, as the filter relies on a fixed estimated covariance $\hat{\mathbf{R}}$ while the true covariance \mathbf{R} changes over time. The conventional MMSE estimator suffers from an unavoidable performance penalty due to this mismatch, quantified as

$$\Delta_{\text{mis}} = \left\| \left(\mathbf{W}_{\text{mis}} - \mathbf{W}^* \right)_{\Sigma_{yy}}^{1/2} \right\|_F^2 \geq 0. \quad (37)$$

where \mathbf{W}_{mis} denotes the mismatched filter and \mathbf{W}^* represents the oracle MMSE filter with perfect covariance knowledge. As

detailed in Appendix B, this penalty is proportional to $\|\Delta\mathbf{R}\|_F^2$ and establishes a fundamental performance floor, particularly severe in high-mobility scenarios such as TDL-D and TDL-E.

In contrast, A-MMSE learns the optimal filter directly from data without explicit covariance estimation, bypassing the mismatch problem entirely. The attention mechanism captures true non-stationary channel correlations through an adaptive filter whose error decreases with model capacity and training samples, unlike the fixed penalty Δ_{mis} in conventional MMSE. This fundamental distinction explains A-MMSE's consistent advantage, achieving approximately 43% lower NMSE compared to conventional MMSE across all TDL scenarios.

C. Normalized MSE Comparison

For the channel estimation performance comparison, we present the NMSE across different SNR levels in Fig. 7 and Fig. 8. As shown in the figures, the proposed A-MMSE method consistently achieves the best NMSE performance across all SNR regimes and propagation environments, clearly outperforming the existing SP-based approaches as well as the existing DNN-based approaches. Specifically, the A-MMSE achieves around 43% and 48% lower average NMSE compared to the best SP-based baseline (MMSE) and the best DNN-based baseline (Channelformer), respectively. In the considered TDL models, channel statistics vary from slot to slot, rendering classical MMSE no longer strictly optimal. In this situation, the A-MMSE still achieves significantly lower NMSE than MMSE, where the gains are more pronounced in the TDL-D and TDL-E (high-mobility and mmWave). This advantage arises from that the A-MMSE leverages the powerful learning capability from the Attention Transformer. It is also notable that the proposed A-MMSE outperforms Channelformer, which also employs the Attention Transformer architecture. These gains arise from the novel A-MMSE's two-stage Attention encoder, which first captures frequency-domain correlations and then refines them in the temporal-domain correlation. Crucially, this enables learning the non-stationary channel statistics that vary across OFDM slots more effectively compared to the single-encoder design used in Channelformer.

It is worth noting that the RA-A-MMSE achieves NMSE performance comparable to that of the original A-MMSE, despite its rank reduction. Specifically, in the TDL-B scenario (Fig. 7(a)), the RA-A-MMSE with 10% of rank retains 99.9% of the full-rank A-MMSE, while achieving around 41% lower NMSE than Channelformer. Similar to this, in the TDL-E scenario (Fig. 8) representing mmWave propagation with high frequency selectivity, the RA-A-MMSE with 10% of rank still delivers 99.6% of the full-rank A-MMSE performance and achieves about 25% lower NMSE than Channelformer. These observations highlight the practical advantages of RA-A-MMSE. It preserves the high estimation accuracy of A-MMSE while enabling substantial complexity reduction via rank adaptation.

D. BER Performance Analysis

To evaluate the impact of channel estimation accuracy on symbol detection performance, we examine the BER per-

formance for 16-QAM modulation in the TDL-E scenario. Fig. 9 presents the BER curves for the challenging mmWave channel environment. The results reveal distinct performance characteristics at different SNR regimes. At low SNRs (0 - 10 dB), all methods exhibit similar BER performance, as the noise dominates the overall system performance. However, at high SNRs (20 - 30 dB), where channel estimation accuracy becomes the limiting factor, the A-MMSE demonstrates substantial gains. At 25 dB, the A-MMSE achieves a BER of 8.59×10^{-5} compared to 9.89×10^{-5} for MMSE and 1.17×10^{-4} for Channelformer, representing improvements of 13.1% and 26.6% respectively. These BER results confirm that the superior channel estimation accuracy of A-MMSE directly translates to enhanced symbol detection performance, with benefits becoming increasingly significant in high SNR.

E. Robustness to SNR Mismatch

To evaluate the robustness and generalization of the proposed A-MMSE under SNR mismatch conditions, we consider three independent models trained at SNR values of 0 dB, 15 dB, and 30 dB, and evaluate each model across the entire SNR range of 0 - 30 dB. Fig. 10 and Fig. 11(a) illustrate the NMSE performance of A-MMSE across the TDL-B, TDL-D, and TDL-E scenarios, respectively.

Across all considered channel profiles, the A-MMSE with SNR mismatch reveals a consistent trend. For instance, the A-MMSE model trained at 0 dB collapses when the test SNR increases. This is mainly because the overwhelming noise obscures the channel's latent statistics, causing the Attention Transformer to memorize a denoiser rather than learn the true optimal filter. In contrast, the A-MMSE models trained at 15 dB and 30 dB generalize effectively to unseen SNR levels. Specifically, in TDL-B, the 15 dB model retains 99.8% and the 30 dB model retains 99.3% of the no-mismatch reference performance. In TDL-D, the corresponding performance retentions are 99.1% and 98.1%, and in TDL-E, they are 99.0% and 98.1%, respectively.

The persistent advantage of the (15) dB model stems from a sweet-spot effect, where moderate noise serves as regularization, allowing the network to internalize the full MMSE filter structure without overfitting to noise-free conditions. At (30) dB, the regularization effect becomes nearly negligible, resulting in slight robustness loss as operating conditions deviate from the training SNR.

F. Performance-Complexity Trade-off

In this subsection, we evaluate computational complexity of each channel estimation method in terms of floating-point operations (FLOPs). FLOPs quantify the number of arithmetic operations required for inference (i.e., channel estimation). For example, one complex multiplication consists of four real multiplications and two real additions, totaling six real FLOPs. We note that training complexity is not considered in this analysis, as it is performed offline and has little impact on the real-time inference costs during deployment.

Fig. 11(b) illustrates the trade-off between the average NMSE and computational complexity across all evaluated

TABLE II
FLOPS COMPARISON FOR CHANNEL ESTIMATION
($K = 10^3$, $M = 10^6$, $G = 10^9$)

Method	Computational Cost (FLOPs)	
# of Pilots	$L=36$	$L=72$
MMSE	$\approx 11\text{M}$	$\approx 21\text{M}$
1D-MMSE	$\approx 21\text{K}$	$\approx 41\text{K}$
LS	$\approx 7.5\text{K}$	$\approx 15\text{K}$
ChannelNet	$\approx 1.35\text{G}$	$\approx 1.35\text{G}$
Channelformer	$\approx 10\text{M}$	$\approx 21\text{M}$
A-MMSE	$\approx 5.8\text{K}$	
RA-A-MMSE	$\approx 8608r$, $r = \text{rank}$	

TDL channel models. We also summarize the per-inference FLOPs for all the considered methods in Table II. As shown in Fig. 11(b), the proposed A-MMSE achieves superior channel estimation performance with substantially lower computational complexity. Specifically, it yields around 46.3% lower average NMSE and 95.1% fewer FLOPs compared to the average performance of MMSE and Channelformer. The RA-A-MMSE, which incorporates rank adaptation, further reduces complexity with minimal performance loss, consistently outperforming existing approaches.

As discussed earlier, these benefits arise from the fact that A-MMSE relies solely on computationally efficient linear operations during channel estimation. Remarkably, the A-MMSE and the RA-A-MMSE push the boundaries of the performance–complexity trade-off, achieving a new level of estimation accuracy at drastically reduced computational cost. This shift sets a new state-of-the-art for practical channel estimation by redefining the achievable balance between accuracy and efficiency.

G. Performance Comparison to Sensing-aided Estimation

Recent sensing-aided channel estimation methods present significant trade-offs compared to the A-MMSE framework, particularly in high-mobility scenarios like TDL-D. The sensing-aided approach requires a complex multi-stage processing pipeline for echo analysis, adding considerable computational overhead. Unlike this, A-MMSE performs channel estimation through a single, efficient linear operation. Moreover, sensing-aided techniques depend critically on echo signal quality, a vulnerability absent in A-MMSE, which maintains consistent performance without auxiliary information. In Fig. 12, we also compare the channel estimation performance between our A-MMSE and the sensing-aided approach. At 15 dB SNR in TDL-D, A-MMSE achieves an NMSE of 3.26×10^{-3} , outperforming the sensing-aided approach (5.01×10^{-3}) by 35%. This performance gap widens at higher SNRs, where sensing-aided methods plateau while A-MMSE continues to improve. It demonstrates that data-driven learning overcomes the fundamental limitations of echo-based refinement. These results indicate that A-MMSE retains its advantage even without relying on explicit echo information, highlighting its robustness and applicability.

VII. CONCLUSION

In this paper, we proposed the A-MMSE method for OFDM channel estimation. Our key idea is to integrate the classi-

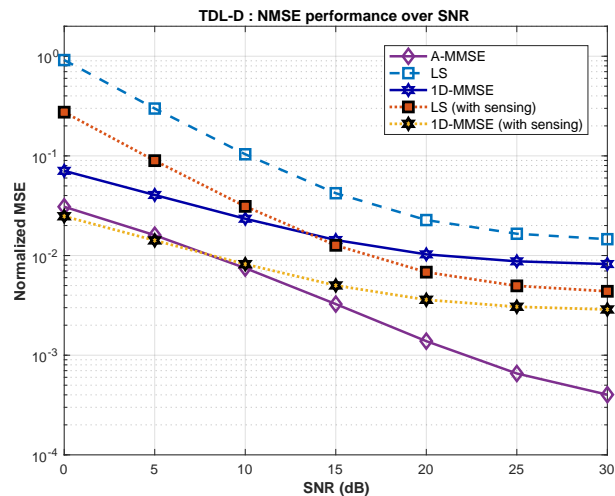


Fig. 12. A-MMSE vs. Sensing-aided channel estimation

cal SP-based framework with the learning capability of the DNN-based approach. Specifically, the proposed A-MMSE learns the linear filtering matrix via the Attention Transformer and applies it for channel estimation, achieving both high estimation accuracy and substantial computational efficiency. In particular, to enhance the learning of the linear filtering matrix, we developed a novel two-stage Attention encoder that effectively captures the frequency and temporal correlation structures of the OFDM channel. Building on this architecture, we further introduced a rank-adaptive extension of A-MMSE, referred to as the RA-A-MMSE. The RA-A-MMSE stands out by dynamically adjusting the rank of the linear filtering matrix, thereby controlling the computational overhead associated with channel estimation. Through extensive numerical simulations using 3GPP TDL channel models, we demonstrated that the proposed A-MMSE provides significant performance gains in channel estimation compared to conventional SP-based methods (e.g., LS and MMSE) as well as DNN-based methods (e.g., ChannelNet [9] and Channelformer [15]). We further showed that the RA-A-MMSE effectively balances estimation performance and computational complexity, offering substantial reductions in computational overhead with minimal performance degradation.

The proposed A-MMSE and the RA-A-MMSE frameworks offer several key advantages: i) once trained, only the linear filter is used, resulting in architectural simplicity; ii) by leveraging the learning capability of the Attention Transformer, it adapts effectively to diverse channel conditions; and iii) it provides a principled integration of classical signal processing with deep learning. With its modular design and computational efficiency, the A-MMSE aligns well with emerging 6G physical layer design principles. Its integration of data-driven learning with model-based filtering makes it well-suited for standardization in scalable, low-complexity, and AI-native wireless transceiver design. Consequently, the proposed architecture offers a practical pathway toward learning-enhanced, standards-compliant channel estimation in next-generation wireless systems. Future work could explore a promising hybrid model that integrates the A-MMSE frame-

work with sensing-aided approaches, while also developing a practical ground-truth-free training methodology using Ridge regression. These advancements would lay the groundwork for a fully online A-MMSE framework that can adapt in real-time to dynamic wireless environments without perfect channel knowledge.

APPENDIX A PROOF OF KRONECKER PRODUCT STRUCTURE

Consider the time-varying channel impulse response $h(t, \tau)$ [39] with time-frequency transfer function

$$L_H(t, f) = \int_{-\infty}^{\infty} h(t, \tau) e^{-j2\pi f \tau} d\tau. \quad (38)$$

Under WSSUS [39]: $\mathbb{E}[h(t, \tau)h^*(t', \tau')] = r_h(t - t'; \tau)\delta(\tau - \tau')$. This yields 2D stationarity:

$$\mathbb{E}[L_H(t, f)L_H^*(t', f')] \quad (39)$$

$$= \iint \mathbb{E}[h(t, \tau)h^*(t', \tau')] e^{-j2\pi f \tau} e^{j2\pi f' \tau'} d\tau d\tau' \quad (40)$$

$$= \int r_h(t - t'; \tau) e^{-j2\pi(f - f')\tau} d\tau. \quad (41)$$

Setting $\Delta t = t' - t$, $\Delta f = f' - f$, then we have $\mathbb{E}[L_H(t, f)L_H^*(t + \Delta t, f + \Delta f)] = R_H(\Delta t, \Delta f)$. This correlation function and scattering function form a 2D Fourier pair:

$$R_H(\Delta t, \Delta f) = \int_{-\infty}^{\infty} \int_{-\infty}^{\infty} C_H(\tau, \nu) e^{j2\pi(\nu \Delta t - \tau \Delta f)} d\tau d\nu. \quad (42)$$

Assuming separable scattering [35] $C_H(\tau, \nu) = P_\tau(\tau) \cdot S_\nu(\nu)$, we can substitute as

$$R_H(\Delta t, \Delta f) = \int_{-\infty}^{\infty} \int_{-\infty}^{\infty} P_\tau(\tau) S_\nu(\nu) e^{j2\pi(\nu \Delta t - \tau \Delta f)} d\tau d\nu \quad (43)$$

$$= \int_{-\infty}^{\infty} P_\tau(\tau) e^{-j2\pi \tau \Delta f} d\tau \cdot \int_{-\infty}^{\infty} S_\nu(\nu) e^{j2\pi \nu \Delta t} d\nu \quad (44)$$

$$= r_t(\Delta t) \cdot r_f(\Delta f). \quad (45)$$

For OFDM with N subcarriers and M symbols: $H[n, m] = L_H(mT_{sym}, n\Delta f_s)$. The discrete correlation: $\mathbb{E}[H[n, m]H^*[n', m']] = r_t[(m - m')T_{sym}] \cdot r_f[(n - n')\Delta f_s]$. Define frequency and temporal correlation matrices as

- $[\mathbf{R}_f]_{n, n'} = r_f[(n - n')\Delta f_s] \in \mathbb{C}^{N \times N}$
- $[\mathbf{R}_t]_{m, m'} = r_t[(m - m')T_{sym}] \in \mathbb{C}^{M \times M}$

For vectorized channel $\mathbf{h} = \text{vec}(\mathbf{H})$ with $h_{n+mN} = H[n, m]$, OFDM channel's correlation can be represented

$$[\mathbf{R}]_{(n+mN), (n'+m'N)} = \mathbb{E}[H[n, m]H^*[n', m']] \quad (46)$$

$$= [\mathbf{R}_t]_{m, m'} \cdot [\mathbf{R}_f]_{n, n'}. \quad (47)$$

Therefore $\mathbf{R} = \mathbb{E}[\mathbf{h}\mathbf{h}^H] = \mathbf{R}_t \otimes \mathbf{R}_f$.

APPENDIX B PERFORMANCE PENALTY OF COVARIANCE-MISMATCHED MMSE

In this appendix, we provide a rigorous mathematical analysis of the performance penalty incurred by covariance-mismatched MMSE estimation. The oracle MMSE filter, assuming perfect knowledge of the true channel covariance \mathbf{R} , is given by

$$\mathbf{W}^* = \Sigma_{xy} \Sigma_{yy}^{-1} = \mathbf{R}\mathbf{S}^H \left(\mathbf{S}\mathbf{R}\mathbf{S}^H + \sigma^2 \mathbf{I} \right)^{-1}. \quad (48)$$

where \mathbf{S} denotes the pilot selection matrix, $\Sigma_{xy} = \mathbf{R}\mathbf{S}^H$ is the cross-covariance between the full channel and pilot observations, and $\mathbf{S}\mathbf{R}\mathbf{S}^H + \sigma^2 \mathbf{I}$ is the auto-covariance of pilot observations. The corresponding minimum achievable MSE is

$$\text{MSE}(\mathbf{W}^*) = \text{tr}(\mathbf{R}) - \text{tr}(\Sigma_{xy} \Sigma_{yy}^{-1} \Sigma_{yx}). \quad (49)$$

In practice, we must rely on an estimated or surrogate covariance $\tilde{\mathbf{R}}$, leading to the mismatched filter

$$\mathbf{W}_{\text{mis}} = \tilde{\mathbf{R}}\mathbf{S}^H \left(\mathbf{S}\tilde{\mathbf{R}}\mathbf{S}^H + \sigma^2 \mathbf{I} \right)^{-1}. \quad (50)$$

The performance of this mismatched filter is strictly worse than the oracle, with total MSE given by

$$\text{MSE}(\mathbf{W}_{\text{mis}}) = \text{MSE}(\mathbf{W}^*) + \Delta_{\text{mis}}. \quad (51)$$

where $\Delta_{\text{mis}} \geq 0$ represents the irreducible penalty due to covariance mismatch. The penalty term can be explicitly quantified as

$$\Delta_{\text{mis}} = \left\| (\mathbf{W}_{\text{mis}} - \mathbf{W}^*) \Sigma_{yy}^{1/2} \right\|_F^2 \geq 0. \quad (52)$$

To prove this, we expand the MSE of the mismatched filter:

$$\text{MSE}(\mathbf{W}_{\text{mis}}) = \mathbb{E} \left[\left\| \mathbf{H} - \mathbf{W}_{\text{mis}} \mathbf{y}_p \right\|_2^2 \right]. \quad (53)$$

where \mathbf{H} is the true channel vector and \mathbf{y}_p is the pilot observation vector. By adding and subtracting $\mathbf{W}^* \mathbf{y}_p$, we obtain

$$\text{MSE}(\mathbf{W}_{\text{mis}}) = \mathbb{E} \left[\left\| (\mathbf{H} - \mathbf{W}^* \mathbf{y}_p) + (\mathbf{W}^* - \mathbf{W}_{\text{mis}}) \mathbf{y}_p \right\|_2^2 \right]. \quad (54)$$

Using the orthogonality principle of the optimal MMSE estimator, the cross term vanishes, yielding

$$\text{MSE}(\mathbf{W}_{\text{mis}}) = \text{MSE}(\mathbf{W}^*) + \mathbb{E} \left[\left\| (\mathbf{W}^* - \mathbf{W}_{\text{mis}}) \mathbf{y}_p \right\|_2^2 \right]. \quad (55)$$

The second term can be written as

$$\Delta_{\text{mis}} = \text{tr} \left((\mathbf{W}_{\text{mis}} - \mathbf{W}^*) \Sigma_{yy} (\mathbf{W}_{\text{mis}} - \mathbf{W}^*)^H \right). \quad (56)$$

which is equivalent to $\Delta_{\text{mis}} = \left\| (\mathbf{W}_{\text{mis}} - \mathbf{W}^*) \Sigma_{yy}^{1/2} \right\|_F^2 \geq 0$.

For small covariance mismatches $\Delta \mathbf{R} = \tilde{\mathbf{R}} - \mathbf{R}$, we can establish a local quadratic lower bound. Let $\tilde{\Sigma}_{yy} = \mathbf{S}\tilde{\mathbf{R}}\mathbf{S}^H + \sigma^2 \mathbf{I}$, and $\Delta \Sigma_{yy} = \tilde{\Sigma}_{yy} - \Sigma_{yy} = \mathbf{S}\Delta \mathbf{R}\mathbf{S}^H$. Using first-order perturbation analysis of the matrix inverse, we have

$$\mathbf{W}_{\text{mis}} - \mathbf{W}^* \approx \Delta \mathbf{R}\mathbf{S}^H \Sigma_{yy}^{-1} - \mathbf{R}\mathbf{S}^H \Sigma_{yy}^{-1} \Delta \Sigma_{yy} \Sigma_{yy}^{-1}. \quad (57)$$

Substituting $\Delta \Sigma_{yy} = \mathbf{S}\Delta \mathbf{R}\mathbf{S}^H$ and simplifying as

$$\mathbf{W}_{\text{mis}} - \mathbf{W}^* \approx (\mathbf{I} - \mathbf{W}^* \mathbf{S}) \Delta \mathbf{R}\mathbf{S}^H \Sigma_{yy}^{-1}. \quad (58)$$

Therefore, the mismatch penalty satisfies

$$\Delta_{\text{mis}} \geq \lambda_{\min}(\Sigma_{yy}) \left\| (\mathbf{I} - \mathbf{W}^* \mathbf{S}) \Delta \mathbf{R} \mathbf{S}^H \Sigma_{yy}^{-1/2} \right\|_F^2. \quad (59)$$

Using the matrix norm property $\|\mathbf{AB}\|_F \geq \sigma_{\min}(\mathbf{A})\|\mathbf{B}\|_F$, where σ_{\min} denotes the smallest singular value of a matrix, we obtain

$$\Delta_{\text{mis}} \geq \lambda_{\min}(\Sigma_{yy}) \sigma_{\min}^2(\mathbf{I} - \mathbf{W}^* \mathbf{S}) \sigma_{\min}^2(\mathbf{S}) \left\| \Sigma_{yy}^{-1/2} \Delta \mathbf{R} \right\|_F^2. \quad (60)$$

Further, noting that $\left\| \Sigma_{yy}^{-1/2} \Delta \mathbf{R} \right\|_F^2 \geq \frac{\|\Delta \mathbf{R}\|_F^2}{\rho_s^2 \|\mathbf{R}\|_2 + \sigma^2}$ for \mathbf{S} with a bounded spectral norm $\rho_s = \|\mathbf{S}\|_2$, we establish the quadratic lower bound

$$\Delta_{\text{mis}} \geq \lambda_{\min}(\Sigma_{yy}) c^2 \|\Delta \mathbf{R}\|_F^2, \quad (61)$$

where $c = \frac{\sigma_{\min}(\mathbf{I} - \mathbf{W}^* \mathbf{S}) \sigma_{\min}(\mathbf{S})}{\rho_s^2 \|\mathbf{R}\|_2 + \sigma^2} > 0$ is a positive constant dependent on the system parameters. Even small covariance estimation errors result in an irreducible quadratic performance penalty for conventional signal processing methods.

REFERENCES

- [1] M. Shafi, A. F. Molisch, P. J. Smith, T. Haustein, P. Zhu, P. De Silva, F. Tufvesson, A. Benjebbour, and G. Wunder, "5G: A tutorial overview of standards, trials, challenges, deployment, and practice," *IEEE J. Sel. Areas Commun.*, vol. 35, no. 6, pp. 1201–1221, 2017.
- [2] P. Guan, D. Wu, T. Tian, J. Zhou, X. Zhang, L. Gu, A. Benjebbour, M. Iwabuchi, and Y. Kishiyama, "5G field trials: OFDM-based waveforms and mixed numerologies," *IEEE J. Sel. Areas Commun.*, vol. 35, no. 6, pp. 1234–1243, 2017.
- [3] S. D. Liyanaarachchi, T. Riihonen, C. B. Barneto, and M. Valkama, "Optimized waveforms for 5G–6G communication with sensing: Theory, simulations and experiments," *IEEE Trans. Wireless Commun.*, vol. 20, no. 12, pp. 8301–8315, 2021.
- [4] O. Edfors, M. Sandell, J.-J. van de Beek, S. Wilson, and P. Borjesson, "OFDM channel estimation by singular value decomposition," *IEEE Trans. Commun.*, vol. 46, no. 7, pp. 931–939, 1998.
- [5] Y. Li, "Pilot-symbol-aided channel estimation for OFDM in wireless systems," *IEEE Trans. Veh. Technol.*, vol. 49, no. 4, pp. 1207–1215, 2000.
- [6] Y. Liu, Z. Tan, H. Hu, L. J. Cimini, and G. Y. Li, "Channel estimation for OFDM," *IEEE Commun. Surveys & Tutorials*, vol. 16, no. 4, pp. 1891–1908, 2014.
- [7] C. Qing, W. Hu, Z. Liu, G. Ling, X. Cai, and P. Du, "Sensing-aided channel estimation in ofdm systems by leveraging communication echoes," *IEEE Internet of Things Journal*, vol. 11, no. 23, pp. 38 023–38 039, 2024.
- [8] X. Chen, Z. Feng, J. Andrew Zhang, Z. Wei, X. Yuan, and P. Zhang, "Sensing-aided uplink channel estimation for joint communication and sensing," *IEEE Wireless Communications Letters*, vol. 12, no. 3, pp. 441–445, 2023.
- [9] M. Soltani, V. Pourahmadi, A. Mirzaei, and H. Sheikhzadeh, "Deep learning-based channel estimation," *IEEE Commun. Lett.*, vol. 23, no. 4, pp. 652–655, 2019.
- [10] L. Li, H. Chen, H.-H. Chang, and L. Liu, "Deep residual learning meets OFDM channel estimation," *IEEE Wireless Commun. Lett.*, vol. 9, no. 5, pp. 615–618, 2020.
- [11] D. Luan and J. Thompson, "Low complexity channel estimation with neural network solutions," in *Proc. 25th International ITG Workshop on Smart Antennas (WSA)*, 2021, pp. 1–6.
- [12] E. Balevi, A. Doshi, A. Jalal, A. Dimakis, and J. G. Andrews, "High dimensional channel estimation using deep generative networks," *IEEE J. Sel. Areas Commun.*, vol. 39, no. 1, pp. 18–30, 2021.
- [13] A. Vaswani, N. Shazeer, N. Parmar, J. Uszkoreit, L. Jones, A. N. Gomez, Ł. Kaiser, and I. Polosukhin, "Attention is all you need," *arXiv preprint arXiv:1706.03762*, 2017.
- [14] J. Li, R. Wang, Y. Yuan, W. Zheng, B. He, and M. Li, "Wireless channel estimation based on transformer and super-resolution," 2023.
- [15] D. Luan and J. S. Thompson, "Channelformer: Attention based neural solution for wireless channel estimation and effective online training," *IEEE Trans. Wireless Commun.*, vol. 22, no. 10, pp. 6562–6577, 2023.
- [16] V. Nair and G. E. Hinton, "Rectified linear units improve restricted boltzmann machines," in *Proceedings of the International Conference on Machine Learning (ICML)*, 2010, pp. 807–814.
- [17] Y. LeCun, L. Bottou, G. B. Orr, and K. R. Müller, "Efficient backprop," in *Neural Networks: Tricks of the Trade*. Springer, 2012, pp. 9–48.
- [18] D. A. Clevert, T. Unterthiner, and S. Hochreiter, "Fast and accurate deep network learning by exponential linear units (ELUs)," *arXiv preprint arXiv:1511.07289*, 2015.
- [19] D. Scherer, A. Müller, and S. Behnke, "Evaluation of pooling operations in convolutional architectures for object recognition," in *Artificial Neural Networks–ICANN 2010*. Springer, 2010, pp. 92–101.
- [20] I. Greenberg, N. Yannay, and S. Mannor, "Optimization or architecture: How to hack Kalman filtering," in *Proc. of the Int. Conf. on Neural Information Processing Systems (NeurIPS)*, 2023.
- [21] L. V. Nguyen, N. T. Nguyen, N. H. Tran, M. Juntti, A. L. Swindlehurst, and D. H. N. Nguyen, "Leveraging deep neural networks for massive MIMO data detection," *IEEE Wireless Commun.*, vol. 30, no. 1, pp. 174–180, 2023.
- [22] N. Shlezinger and Y. C. Eldar, "Model-based deep learning," *Foundations and Trends® in Signal Processing*, vol. 17, no. 4, pp. 291–416, 2023.
- [23] G. Revach, N. Shlezinger, X. Ni, A. L. Escoriza, R. J. G. van Sloun, and Y. C. Eldar, "KalmanNet: Neural network aided kalman filtering for partially known dynamics," *IEEE Trans. Signal Process.*, vol. 70, pp. 1532–1547, 2022.
- [24] S. Hochreiter and J. Schmidhuber, "Long short-term memory," *Neural Computation*, vol. 9, no. 8, pp. 1735–1780, 1997.
- [25] K. Cho, B. van Merriënboer, C. Gulcehre, D. Bahdanau, F. Bougares, H. Schwenk, and Y. Bengio, "Learning phrase representations using RNN encoder–decoder for statistical machine translation," in *Proc. the Conference on Empirical Methods in Natural Language Process. (EMNLP)*, Oct. 2014, pp. 1724–1734.
- [26] G. Welch and G. Bishop, "An introduction to the Kalman filter," University of North Carolina at Chapel Hill, USA, Tech. Rep., 1995.
- [27] G. Choi, J. Park, N. Shlezinger, Y. C. Eldar, and N. Lee, "Split-KalmanNet: A robust model-based deep learning approach for state estimation," *IEEE Trans. Veh. Technol.*, vol. 72, no. 9, pp. 12 326–12 331, 2023.
- [28] S. Shen, J. Chen, G. Yu, Z. Zhai, and P. Han, "Kalmanformer: Using transformer to model the kalman gain in kalman filters," *Frontiers in Neuroinformatics*, vol. 18, p. 1460255, 2025.
- [29] I. Buchnik, G. Revach, D. Steger, R. J. G. van Sloun, T. Routtenberg, and N. Shlezinger, "Latent-KalmanNet: Learned Kalman filtering for tracking from high-dimensional signals," *IEEE Trans. Signal Process.*, vol. 72, pp. 352–367, 2024.
- [30] N. Shlezinger, G. Revach, A. Ghosh, S. Chatterjee, S. Tang, T. Imbiriba, J. Dunik, O. Straka, P. Closas, and Y. C. Eldar, "AI-aided Kalman filters," *ArXiv Preprint*, 2025.
- [31] Q. Xu, J. Sun, and Z. Xu, "Efficient MU-MIMO beamforming based on majorization-minimization and deep unfolding," *IEEE Trans. Wireless Commun.*, pp. 1–1, 2025.
- [32] L. Pellaco and J. Jaldén, "A matrix-inverse-free implementation of the MU-MIMO WMMSE beamforming algorithm," *IEEE Trans. Signal Process.*, vol. 70, pp. 6360–6375, 2022.
- [33] M. Khani, M. Alizadeh, J. Hoydis, and P. Fleming, "Adaptive neural signal detection for massive MIMO," *IEEE Trans. Wireless Commun.*, vol. 19, no. 8, pp. 5635–5648, 2020.
- [34] S. Coleri, M. Ergen, A. Puri, and A. Bahai, "Channel estimation techniques based on pilot arrangement in OFDM systems," *IEEE Trans. Broadcast.*, vol. 48, no. 3, pp. 223–229, 2002.
- [35] Y. Choi, J. H. Bae, and J. Lee, "Low-complexity 2D LMMSE channel estimation for ofdm systems," in *Proc. IEEE Veh. Technol. Conf.*, 2015, pp. 1–5.
- [36] D. P. Kingma and J. Ba, "Adam: A method for stochastic optimization," *arXiv preprint arXiv:1412.6980*, 2014.
- [37] P. J. Huber, "Robust estimation of a location parameter," *Annals of Mathematical Statistics*, vol. 35, no. 1, pp. 73–101, 1964.
- [38] 3rd Generation Partnership Project (3GPP), "NR; physical channels and modulation," 3GPP, Tech. Rep. TS 38.211, April 2025, release 18. [Online]. Available: https://www.etsi.org/deliver/etsi_ts/138200_138299/138211/18.06.00_60/ts_138211v180600p.pdf
- [39] P. Bello, "Characterization of randomly time-variant linear channels," *IEEE Transactions on Communications Systems*, vol. 11, no. 4, pp. 360–393, 1963.